The electrification and size of jet droplets from bursting bubbles at an air-water interface

Ahmad Ali Joraide

THE ELECTRIFICATION AND SIZE OF JET DROPLETS FROM BURSTING BUBBLES AT AN AIR-WATER INTERFACE.

by

AHMAD ALI JORAIDE,
B. Sc.

PRESENTED IN CANDIDATURE FOR THE DEGREE OF MASTER OF SCIENCE IN THE UNIVERSITY OF DURHAM.

October, 1976.

CONTENTS

ABSTRACT

The work described in this thesis is directed towards a study of the size, height of ejection and electrical charge of jet droplets which are produced from a bursting bubble at an air-liquid interface.

Maximum ejection heights of 12 and 17 cm were obtained for jet droplets of deionized water and sea-water respectively. The ejection height of the top jet droplets were identical for sea-water and deionized water for bubble diameters less than 0.84 mm , in agreement with the results of previous workers. A relation between the top jet droplet diameter, D_d, and the bubble diameter D_B, was found to be of the form $D_d \propto D_B^{1.22}$.

It was found that the natural charge, q, on the jet droplets is related to the droplet radius, r, by the expression $q \propto r^{2.4}$ for a range of droplet radius from 17 up to 65 micrometres. A slow increase in the electric charge of the droplets q with bubble age t followed a relation of $q \propto t^{0.28}$ for a droplet radius of 36 micrometres for tap-water. The top droplet charge increased with decreasing water conductivity and showed reasonable agreement with an electrical double-layer theory proposed by Iribarne and Klemes (1974). The natural charge of the jet droplets was found to be positive over the range of conductivity from about $4 \times 10^4 \mu$ mho's cm^{-1} (sea-water) down to 2.8μmho's cm^{-1} (deionized water). A Faraday cage system was used to measure the electric charge of droplets greater than about 50 micrometres in radius. A decrease in the droplet charge was obtained for droplet radii greater than about 70 micrometres. Possible explanations for

the decrease in charge over the measured droplet radius range from 70 to 140 micrometres are given.

Measurements of the induction charge in jet droplets over a range of induction field from 0 to $\pm$ 175 V cm^{-1} were carried out for both deionized water and sea-water. A linear relation between the jet droplet charge and induction field for top droplet radii from 27 to 76 micrometres and the second jet droplet of radius 50 micrometres was found. The negatively induced charge due to normal fair-weather electric field constitutes only a small fraction of the natural positive charge of jet droplets.

LIST OF FIGURES.

CAPTIONS FOR TABLES.

CHAPTER 1.

GENERAL INTRODUCTION TO DROPLET PRODUCTION BY BURSTING BUBBLES.

1.1. Introduction.

The ejection of small droplets from a bursting bubble was first postulated by Stuhlman (1932). A high speed photographic study by Kientzler et al (1954) confirmed the jet droplet production mechanism. It was shown by both Woodcock et al (1953) and Kientzler et al (1954) that the droplets produced from the jets of bubbles from 40 to 900 micrometres in diameter could produce sea-salt nuclei covering the range of size found by Woodcock (1953) at the level of clouds over the sea. Newitt et al (1954) showed that the generation of droplets by bursting bubbles is influenced by the depth of the bubble below the liquid surface, the bubble diameter and by the temperature and viscosity of the liquid. Blanchard and Woodcock (1957) conclude that the vast majority of the airborn salt nuclei arise from bursting bubbles at the air-sea water interface. They also found that the majority of bubbles are less than about 200 micrometres in diameter. Since the evolution and development of maritime clouds is dependent on the size and number distribution of sea-salt nuclei the physical properties of bubbles and their disintegration products is of much interest to the cloud physicist.

Since it has been found by Woodcock et al (1953) that the droplets produced by the bursting bubbles were electrically charged, bursting bubbles will contribute to the transfer of electric charge between the oceans and the atmosphere. The presence of the electric field in the atmosphere will induce electric charge in the ejected droplets.

Many drop-droplet collisions or coalescence experiments require the use of stable droplet streams. The generation of jet droplets from a bursting bubble at an air-liquid interface provides a wide range of droplet size with known electrical charge - a technique which is quite reproducible. In addition, the production of either a single droplet or a continuous stream of droplets serves as a useful tool in the microphysical study of drop-droplet collision phenomena.

1.2. The mechanism of liquid jet droplet production

When a bubble reaches the surface of a liquid, its upper surface is usually projected above the liquid surface in the form of a hemispherical dome, as shown in Fig.1.1.(b). If the liquid surface contains dissolved salt(s) or is unclean, the bubble may remain on the surface for an appreciable time. Newitt et al (1954) suggest that even in reasonably pure water the time-lag between the bubble reaching the surface and bubble collapse is of the order of 0.01 seconds. The pressure inside the bubble exceeds the surrounding outside pressure by an amount ΔP given by:

$$\Delta P = 4\ T/R. \qquad 1.1.$$

for a hemispherical upper dome (Fig.1.1.(b)); where T is the surface tension of the liquid and R is the bubble radius.

High speed photography has been used by some workers, including Woodcock et al (1953), Kientzler et al (1954) and Newitt et al (1954) to elucidate the mechanism of bubble collapse and the resultant droplet formation. The sequence of events in the bubble burst process is outlined in Fig.1.1. from photographic evidence of Newitt et al (1954). The excess internal pressure P given by Equation (1.1) extends the interface as shown in Fig.1.1(b), and causes the formation of a secondary cap (Fig.1.1.(c)). This cap disintegrates to form

FIG. 1.1.
MECHANISM OF A BURSTING BUBBLE AT AN AIR-LIQUID INTERFACE.

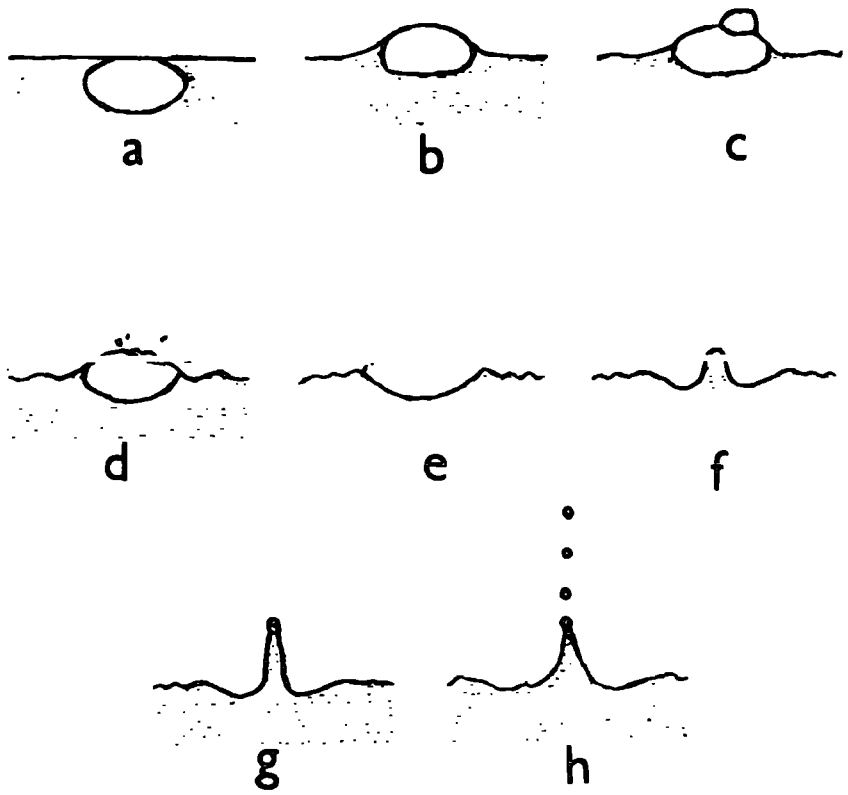

minute droplets (of the order of a few micrometres) which are carried away. The rush of air from the perforated dome sets up a series of standing waves, shown in the figures. The escaping air also results in the formation of a well defined crater (Fig.1.1(e)) in the interface. As the crater fills in, the momentum of the inflowing liquid produces a liquid jet upwards as shown developing in Fig.1.1(f) and (g). The disintegration of the liquid jet filament is associated with the attainment of minimum energy through the formation of spherical droplets, as seen in Fig.1.1(h). The number of jet droplets formed is usually between four and six. The time interval from the initiation of the bubble collapse to the separation of the jet droplets is of the order of a millisecond.

The ejection velocity of the jet droplets increases with decreasing bubble size. Blanchard (1963) computed a top droplet ejection speed of about 20 m sec^{-1} and 10 m sec^{-1} for bubble diameters of 400 and 1,000 micrometres respectively. Blanchard also showed that only the surface free energy of the bubble contributes significantly to the kinetic energy of the droplets. Only about 10 to 20 per cent of the available surface energy is usually converted to kinetic energy, the remainder being dissipated in heat and capillary wave formation.

1.3. <u>The electrification associated with jet droplet production.</u>

Observation of an electric charge on the jet droplets produced from bursting bubbles can be made by allowing the droplets to fall between a pair of electrodes, across which a high d.c. voltage is applied. Blanchard (1955) made the first electric charge measurements on droplets produced at an air-sea water interface. He found that the droplets carried a positive charge. His results suggest that a 20 micrometre diameter droplet possessed a charge of about 1×10^{-7} esu.

The electrification associated with bubble bursting is relevant to the release of charge over the ocean's surface. In addition, the bursting of bubbles in reasonably pure water is of interest since it may be related to the observed electrification of melting ice and snow because large numbers of small air bubbles are released during the melting process. Drake and Mason (1966) showed that the positive charging of the melting ice was greatest when the air bubbles were allowed to burst rapidly at a continuously renewable melt water surface. It is now estimated that separation of electric charge during the melting of ice is a result of the bursting of air bubbles released from the ice during melting.

Since the droplets also acquire a charge due to the presence of ambient or induced electric fields, the electric charge on the droplets can be minimised or practically eliminated by applying a suitable value of induction voltage to the bubble apparatus, as is described in Chapter 2. The work on electric charging of jet droplets will include a study for both the smaller droplet range which has been previously investigated by some workers, notably Blanchard (1963), and to a larger size range up to 200 micrometres in diameter, which has not been previously studied.

1.4. <u>The production of small bubble film droplets.</u>

In addition to the production of the relatively larger jet droplets from bursting bubbles, it is now established, through the study of bubble bursting in a cloud chamber, that the disruption of the bubble cap produces much larger numbers of particles too small to be detected by conventional methods. Mason (1957) found film droplet number concentrations of the order of 200 - 400 per bubble almost independent of diameter. However, Blanchard (1963) using a continuous diffusion chamber, found a decrease in film droplet concentration with decreasing

bubble size and bubbles of diameter less than 200 micrometres produced no film droplets. Blanchard's results were confirmed by the work of Day (1964). The film droplets play an equally important role as jet droplets in acting as condensation centres for cloud droplet production in maritime clouds. However, the work described in this thesis is confined to the study of jet droplets.

1.5. Discussion.

It can be seen from this introductory review of some of the physical processes associated with the production of droplets from the bursting of an air bubble at an air-liquid interface, that there are many aspects of jet droplet production worthy of further investigation. An extension of the work carried out by Blanchard (1963) on the relation between both the size and ejection height of jet droplets as a function of bubble size is described in Chapter 3 of this thesis. In addition, new results on both the size and ejection heights of the second jet droplet are presented.

An investigation of the relation between the natural charge of the jet droplet over a wide range of droplet size from about 35 to 200 micrometres in diameter is carried out. No previous work on droplet charging for droplet size extending beyond about 100 micrometres in diameter has come to the author's attention.

The effect of induction fields varying from 1 to 700 V/cm in the inductive charging of the jet droplets is examined. In addition, the influence of the conductivity of the liquid upon the magnitude of the droplet charge is also studied and compared with prediction.

CHAPTER 2.

THE EXPERIMENTAL APPARATUS AND TECHNIQUES

2.1. Introduction.

This chapter describes the various experimental methods used to study the physical characteristics of the jet droplets produced from bursting bubbles at the air/liquid interface. Firstly, the technique for bubble production is described. A method for the accurate determination of the bubble size is next described. The techniques employed for the measurement of the height of ejection and size of the jet droplets is then described. A description is given of the two techniques used to measure the natural and inductive electric charge of the individual droplets, namely a Millikan Chamber Suspension method and a modified Faraday cage method.

2.2. The method of bubble production.

Both Pyrex capillary and normal glass tubing was used in the production of the bubbles. The glass tubing was heated and drawn out into a fine point. The diameter of the point tip mainly determined the bubble size which, in turn, controlled the jet droplet size. In the following experiments the range of bubble size was varied between 0.19 and 1.5 mm. in radius. A compressed air supply at variable pressure controlled by a bleed off valve from a few psi up to about 30 psi. The capillary tubing was inserted into the liquid reservoir making a slight angle (of the order of 10 degrees) to the horizontal. This was found to give stable and reliable

production of bubbles. The capillary tip was usually immersed in a tall glass beaker. The height of the capillary tip below the liquid surface could be raised from a few mm up to about 28 cm, which gave a variable bubble age from a few tenths of a second up to about 10 seconds.

A schematic diagram of the apparatus used to produce bubbles is shown in Fig.2.1.(a). The tall reservoir was placed in a smaller overflow vessel which was positioned on a variable stand. This proved convenient in order to vary the height of the capillary tip below the liquid level. A supply of liquid was continuously fed to the liquid reservoir in order to renew the liquid surface during the experiments. This helped to maintain the liquid surface free from contaminants and also provided a new surface to the bursting bubble. It was found that bubble-production rate and size was remarkably reproducible for a constant air pressure using the described system. A General Radio 1531 Strobotac was used to determine the bubble frequency. The capillary tips were always cleaned with a dilute solution of chromic acid before use and then rinsed with distilled water. The cleanliness of the tips and of the liquid system in general was a most important factor in determining the reproducibility of experimental results. Glass tubing and accessories were always stored and sealed in polythene bags after use.

In order to produce single bubbles, an apparatus similar to that described by Blanchard (1963) was used. This is shown in Fig.2.2. A stirrer, driven by a variable electric motor in the right hand branch of the apparatus causes the liquid to move in a counter-clockwise direction. Throughout most of the tube, the mean time is only a fraction of a centimetre per second, but as the water moves downward through the 2 mm.

FIG. 2.1(a).
SCHEMATIC DIAGRAM OF THE EXPERIMENTAL APPARATUS FOR BUBBLE AND JET DROPLET PRODUCTION.

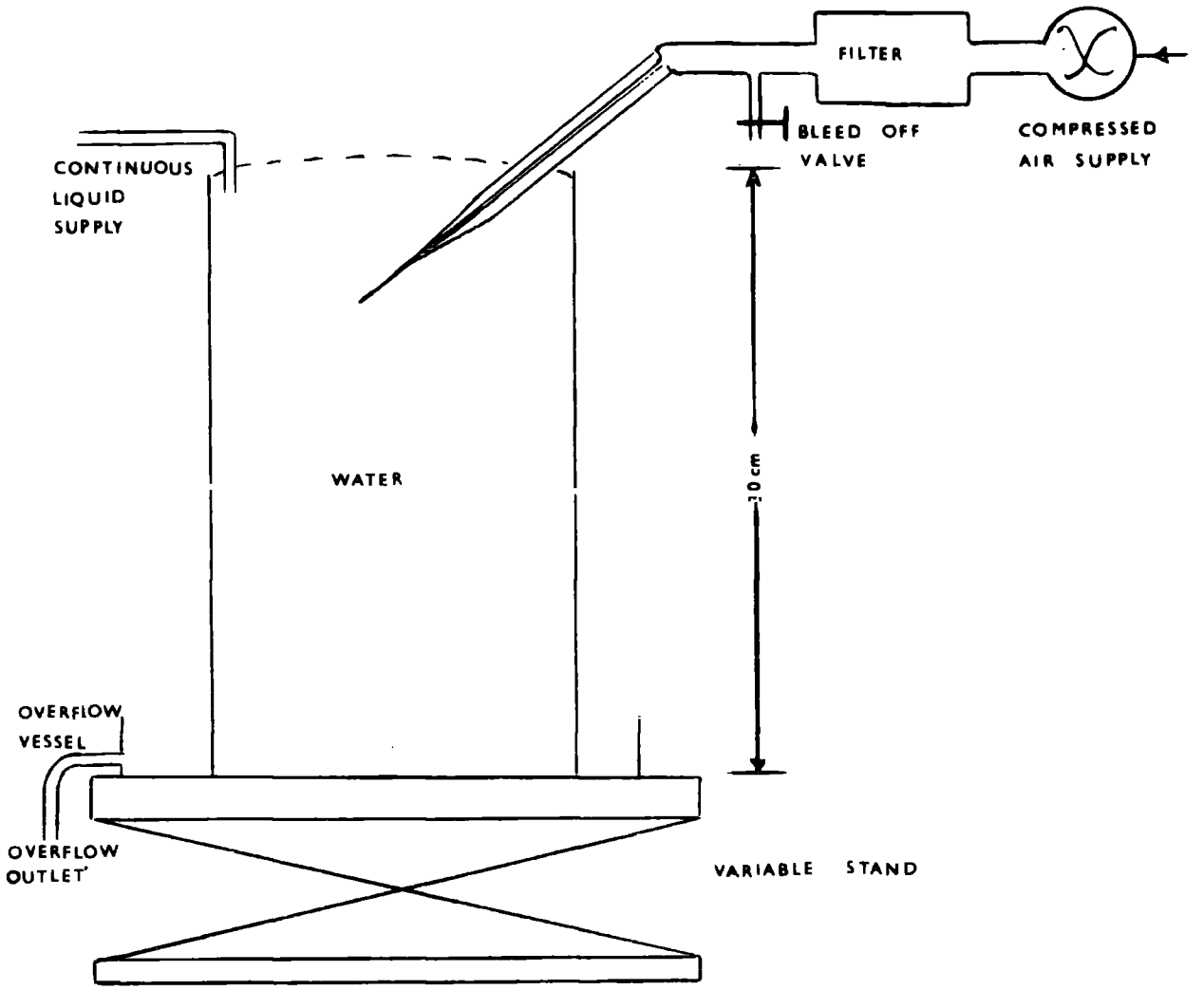

FIG. 2.1(b).
METHOD OF BUBBLE SIZE MEASUREMENT.

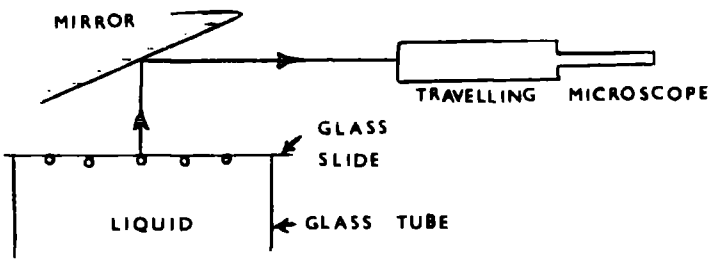

FIG. 2.2.
APPARATUS FOR BUBBLE SUSPENSION.

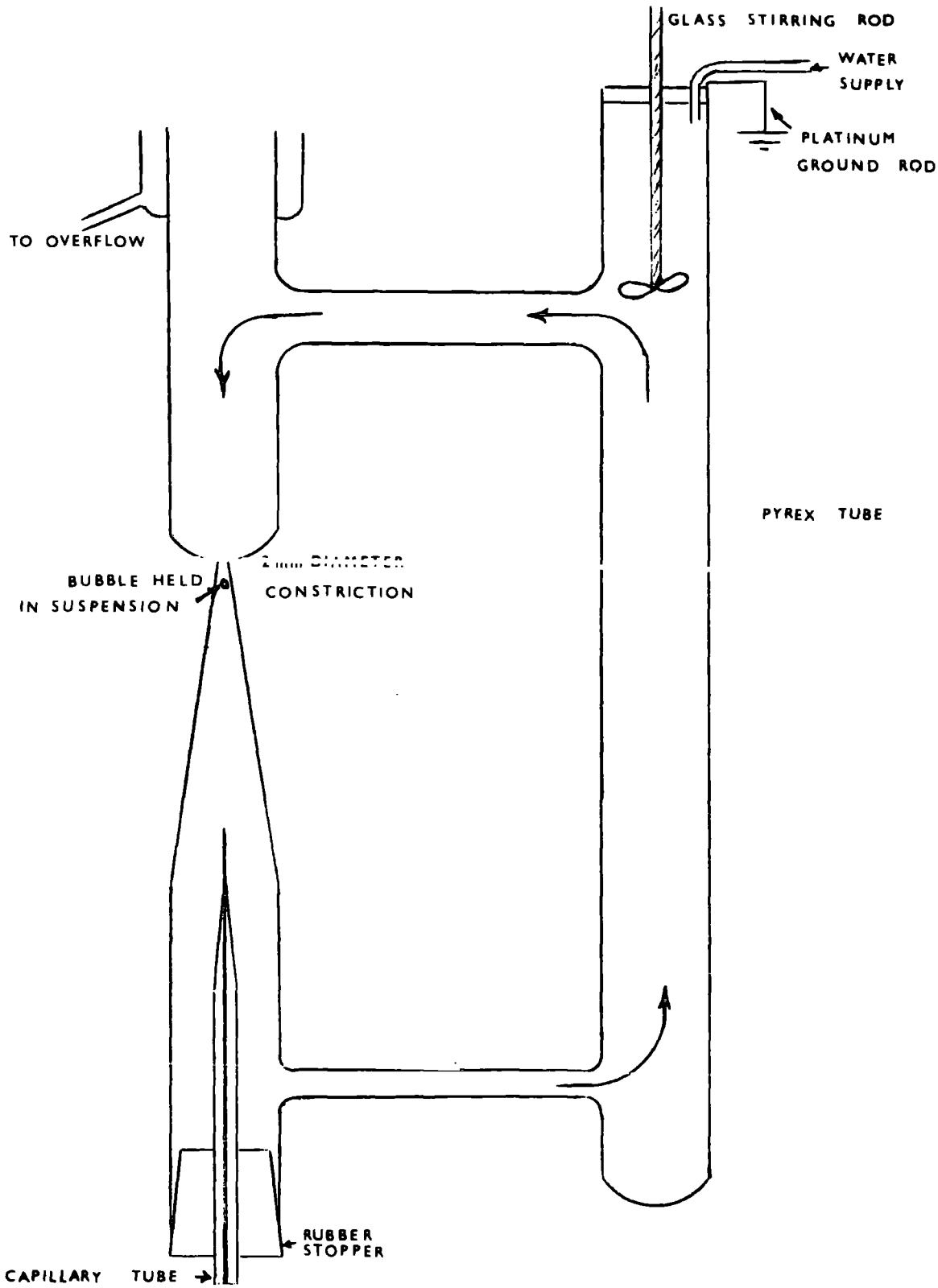

diameter constriction in the left hand branch it accelerates up to several centimetres per second. A bubble released from the capillary tip will rise into the constriction until its rise speed is equal to the downward velocity of the liquid stream. The rate of flow of the downward moving liquid can be controlled by the variable stirring rate and so bubbles over a wide size range can be suspended. The bubble was allowed to rise at any selected time by turning off the stirrer. An overflow reservoir was affixed to the upper left hand branch which allowed for the liquid surface to be continuously renewed. The bubble size could be determined by taking a photograph of the suspended bubble.

A more accurate method for bubble sizing was normally employed using the following technique. The bubbles were trapped beneath a clear glass slide placed across the top of the tube. Consideration of the energy involved suggested that there was no danger of bubbles becoming flattened as was apparent from visual observation. Any bubble disturbance due to gravitational energy will be opposed by the surface free energy which is over two orders of magnitude greater. The bubbles were collected and observed using a mirror system inclined at an angle of 45 degrees, as shown in Fig.2.1.(b). In situ measurement of a number (usually 10-12) of bubbles by means of a travelling microscope yielded an accurate value of the bubble size.

2.3. Jet droplet height and size determination.

The initial formation of the jet droplets produced by the collapse of a bubble at an air/liquid interface cannot be seen by the naked eye but are visible as they reach the top of their trajectory. For large ejection heights, above 3-5 cm. a thin flat insulating plate was mounted horizontally

in a metre rule which was attached to a retort stand. The plate was moved down until the top jet droplet just touched the plate. This was repeated for similarly sized droplets. The experimental technique is shown in Fig.2.3.

An alternative method for determining the ejection height of the jet droplets was also used. The uppermost point of the trajectory of the droplet could be viewed by means of transmitted light from a condenser light system at an angle of about 35 degrees to the straight on position of the droplet. Use was made of a travelling microscope to measure the height of ejection up to a value of about 9 cm.

The size of the jet droplets was determined by measuring the size of the craters made on magnesium coated glass slides, made by the droplets on impaction. This method was first described by May (1950). The droplets were viewed with strong transmitted light with a conventional microscope. Use was made of the knowledge that the droplets usually possess a relatively large positive electric charge in collecting the droplets in the magnesium coated slides. A magnesium coated slide was attached to an electrode which was connected to a large 0 - 15 kv variable negative power supply. The application of a voltage to the electrode caused the droplets to impinge into the magnesium slide under the influence of the electric field.

2.4. The determination of the electric charge of jet droplets.

(a) Millikan type chamber.

An apparatus using the principle of Millikan's classic experiment in the charge of an electron was constructed and used to obtain the charge of the jet droplets produced by the bursting bubbles. This is shown schematically in Fig.2.4.

FIG. 2.3.
TECHNIQUE FOR JET DROPLET HEIGHT DETERMINATION.

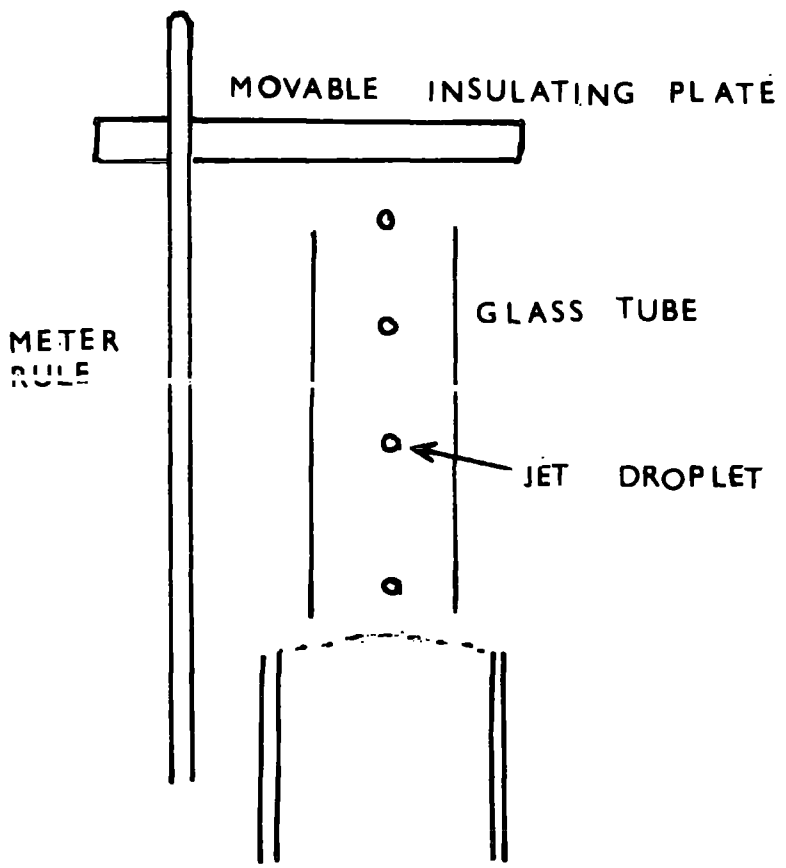

FIG. 2.4.
MILLIKAN TYPE CHAMBER FOR THE DETERMINATION OF THE ELECTRIC CHARGE OF THE JET DROPLETS.

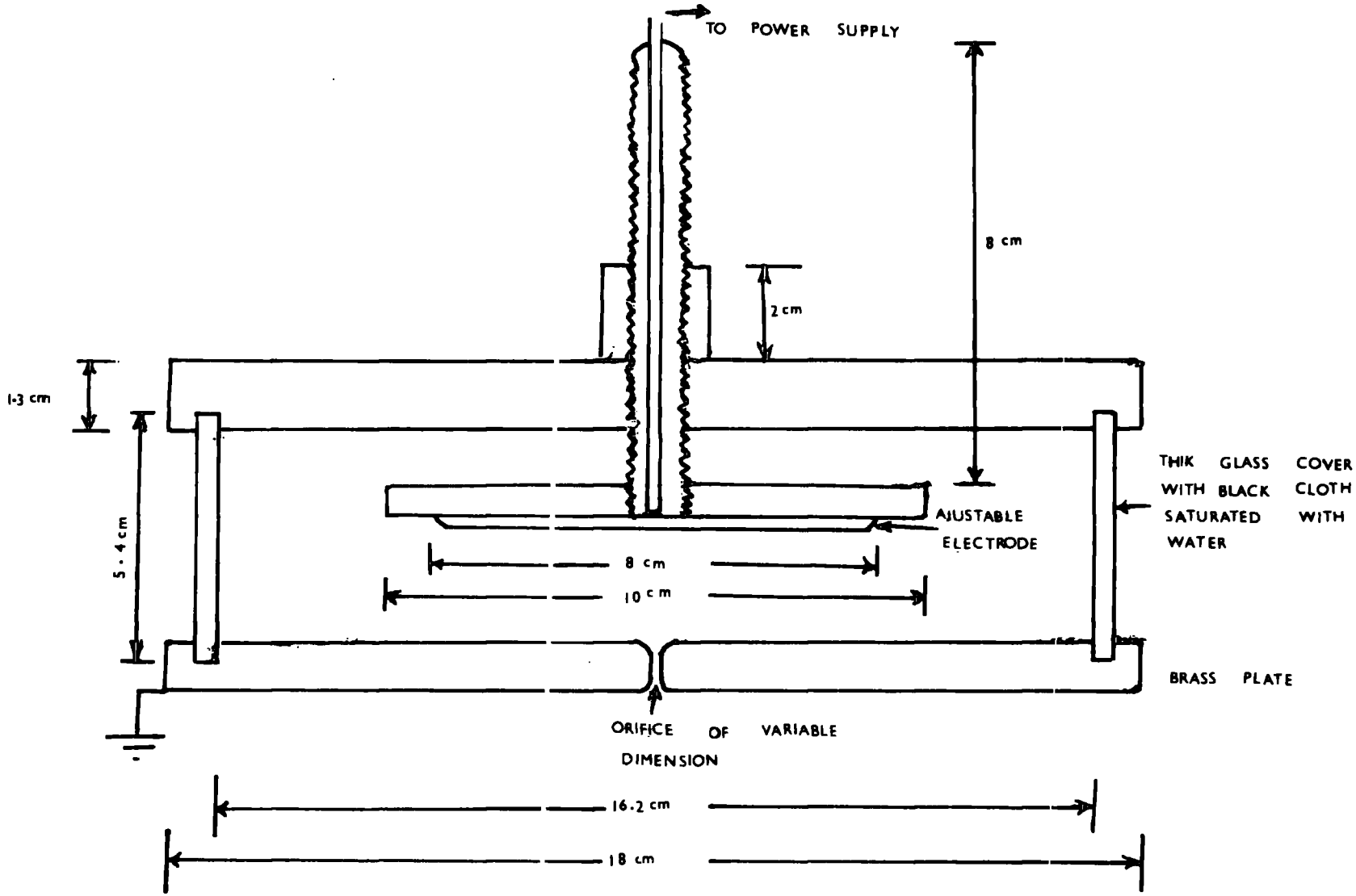

The droplets rose through an orifice whose diameter could be varied, in the centre of an 18 cm. diameter brass base plate on which the Millikan chamber was mounted. The bottom plate was grounded. A circular glass housing sealed off the region from the ambient air. Black felt material attached to the glass enclosure was wetted in order to provide a near saturated environment for the jet droplets and so prevent their evaporation. In addition, the black material facilitated the observation of the jet droplets by masking out unwanted stray light.

The electric field was supplied by means of Brandenburg modular supplies. Models 574 and 645 were used to give negative and positive polarity up to about 15 kv. These modules were driven by a low d.c. power supplies in the range 0 - 30 volts. By monitoring the low voltages on an accurate multimeter (Advance DMM2) the high tension power supplies were calibrated accurately using an electrostatic voltmeter, 0 - 10 kv. range. A calibration curve of negative high voltage with the d.c. power supply voltage is shown in Fig.2.5. The power was attached by means of a high tension cable to an insulated backed electrode, whose inter-electrode distances could be varied. This proved useful since the electric charge of the jet droplets could be independently measured at different electric field spacings.

The jet droplet remains stationary in the electric field when the upward-directed electric force just balances the gravitational force. At this point we can write_

$$4\pi/3\, r^3 \rho g = \text{Eq.} \qquad 2.1.$$

where: r is the drop radius in cm;
ρ is the density of the jet liquid;
g is the acceleration due to gravity;
and E is the electric field in esu cm^{-1}
q is the droplet charge in esu.

In order to determine the drop charge, q, the radius of the drop must also be evaluated independently. The measurement.

FIG. 2.5.
A CALIBRATION CURVE OF NEGATIVE HIGH VOLTAGE.

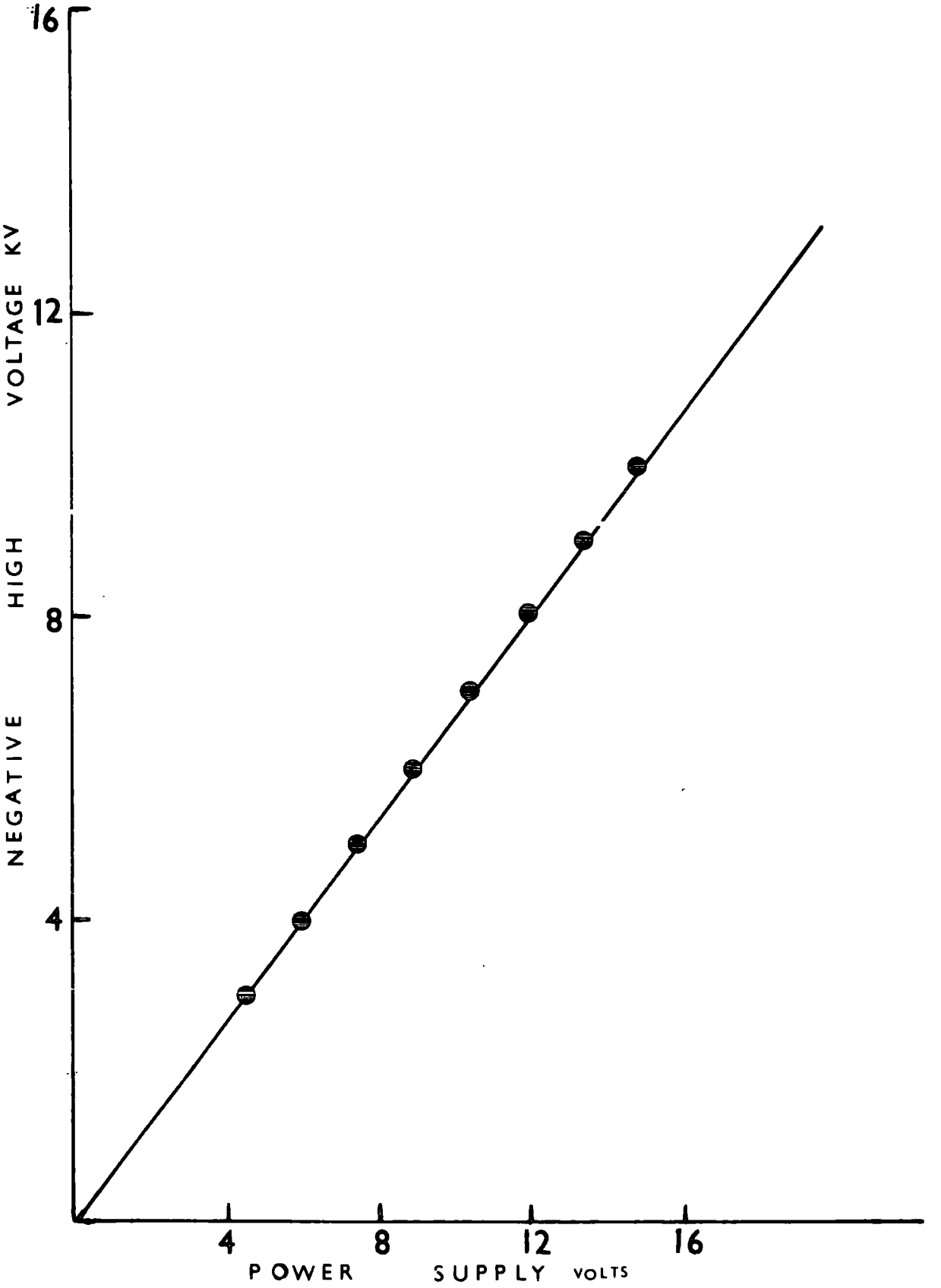

procedure is described in the following chapter.

The Millikan type chamber was adjusted so that the droplets reached their maximum height at about half or two-thirds the distance between the electric field electrodes from the ground electrode plate. The orifice of the base electrode was made sufficiently small ($< 1.5 - 2.0$ mm in diameter) in order to minimize distortion of the electric field lines. The maximum separation, d, between the electrodes was such that the condition of $L/d \gg 3$, where L is the electrode length, in order to preserve the uniformity of the electric field was always assured. The illumination for the jet droplets was provided by a 24 watt microscope lamp and the droplets were viewed at an angle of about 135 degrees from the direction of the light source. A 6" objective telescope assembly was available to view the droplets.

(b) Use of a Faraday cage system.

The Millikan chamber technique used for electric charge determination is limited by the magnitude of the breakdown electric field between the electrode pair, of about 18 kv per cm. This implied that it was not possible, on average, to measure electric charge greater than about 9×10^{-5} esu in jet droplets greater than about 60 micrometres in radius. Therefore a system involving an inverted Faraday cage connected to a sensitive Keithley electrometer Model 602 was used to measure greater quantities of charge on larger jet droplets. A schematic diagram of the apparatus is shown in Fig. 2. 6.

The inner cylinder of the Faraday cage is packed with metal filings so that the ascending jet droplets impinge and make electrical contact with the cylinder, which is electrically connected to a well screened sensitive electrometer. The

FIG. 2.6.
FARADAY CAGE ASSEMBLY FOR THE MEASUREMENT OF THE CHARGE OF LARGER JET DROPLETS.

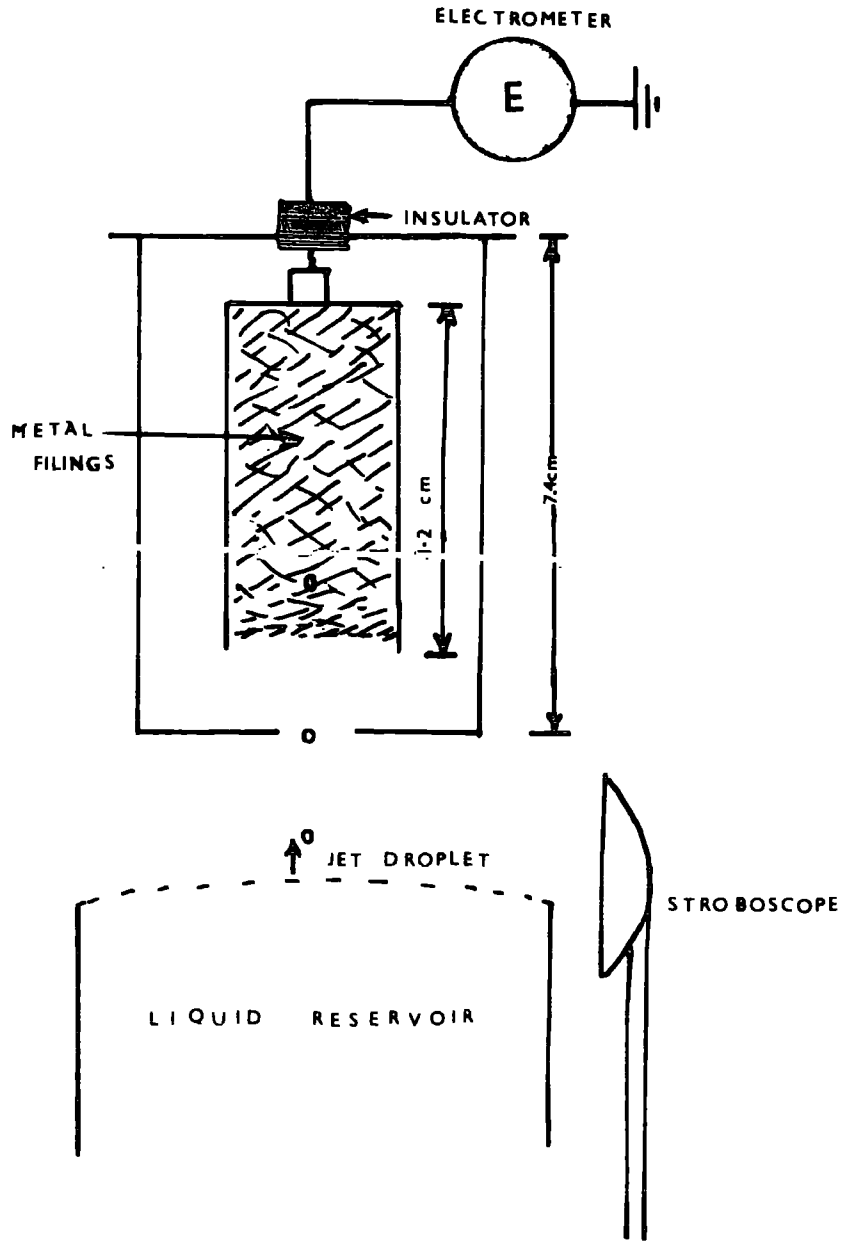

number of jet droplets produced per second was known from the frequency of bubble production determined stroboscopically by a General Radio 1531 Strobotac. The stroboscopic technique proved a reliable and accurate way of knowing the number of jet droplets produced per second. Therefore the electric charge per jet droplet could be readily determined from the constant current reading of the electrometer. This technique proved a good method for the electric charge determination of the larger jet droplets.

The natural charge in the jet droplet is that which the droplet possesses if the jet was formed and had disintegrated in a space free from the influence of electric fields. The conditions for the measurement of the natural charge were obtained by screening the paths of the emerging jet droplets by a metal gauze cylinder which was earthed. This electrostatic metal screen also encircled the liquid reservoir, and extended upwards to the base of the Millikan chamber bottom electrode.

2.5. The induction charge of jet droplets.

The electrostatic screening was removed when measurements of the inductive charging of the jet droplets were made. A brass plate of diameter 7.5cm. was placed at distances varying from 0.5 up to 4 cm. by means of insulating spacers from the grounded plate of the Millikan chamber. The brass plate possessed a central hole of diameter 6 mm through which the droplets passed. A variable d.c. voltage was applied between the brass plate and the grounded plate and the resulting inductive charge on the jet droplets could be measured by either the Millikan suspension chamber (Fig.2.7(a))

FIG. 2.7(a).
EXPERIMENTAL ARRANGEMENT FOR INDUCTIVE CHARGING OF SMALL JET DROPLETS.

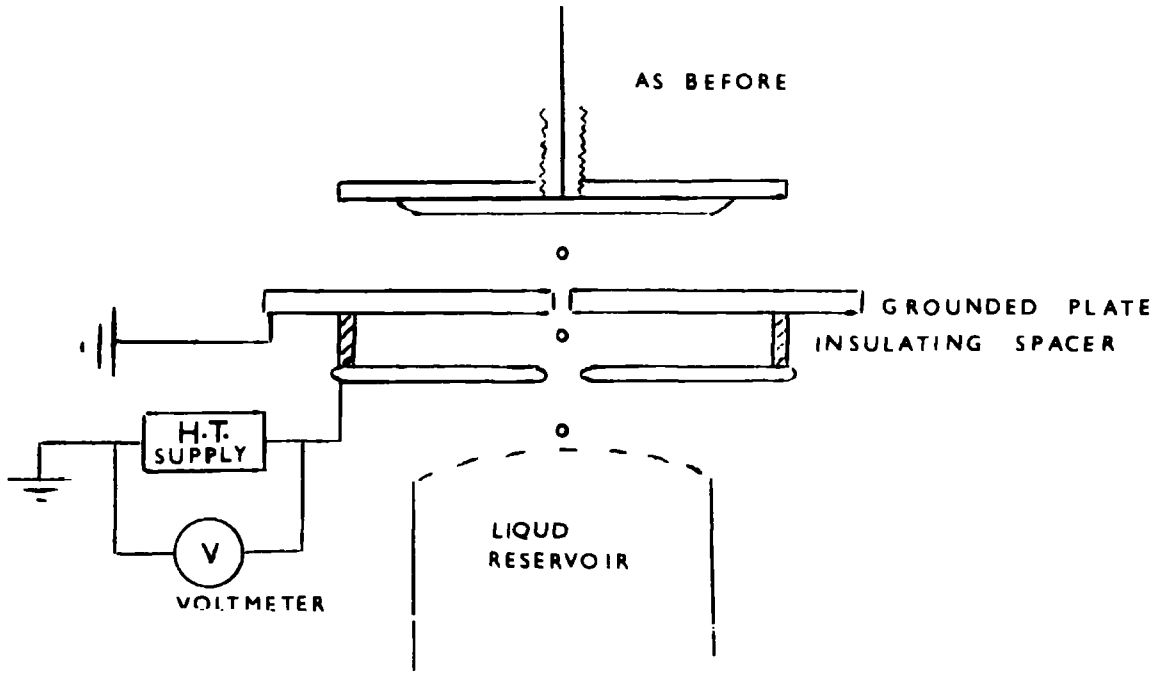

FIG. 2.7(b).
EXPERIMENTAL ARRANGEMENT FOR INDUCTIVE CHARGING OF LARGER JET DROPLETS.

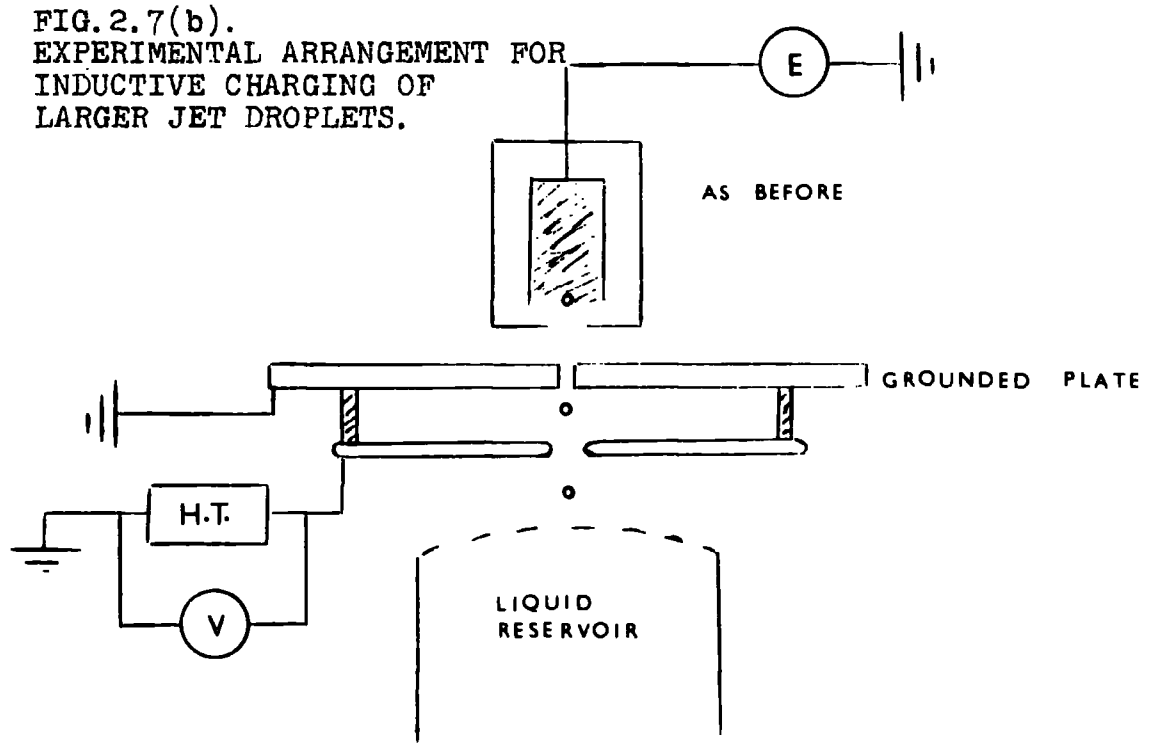

or the Faraday cage technique (Fig.2.7.(b)). A schematic diagram of the assembly used to measure the inductive charge is shown in Fig.2.7(a) and Fig.2.7(b). An accurate Advance DMM2 multimeter was used to measure the applied voltage between the plates. The induction field is given as the magnitude of the voltage applied between the plates divided by the plate spacing. The results of inductive charge experiments are given in Chapter 4.

2.6. Types of water used in the work

Distilled, deionized water, sea water, and solutions of sodium chloride were used in the experiments. Most of the described work was carried out in distilled and deionized water which was contained in a 10 l aspirator and allowed to flow into the cylindrical reservoir at a controlled rate by means of a screwclip where the capillary tubing was positioned. The sea-water was obtained from a remote beach at Ardnamurchan off the west coast of Scotland. The sea-water was carefully filtered through some 15 cm length of glass wool to remove the large plankton. Sea-water contains about 35 gm per litre of sodium chloride. Artificial salt solutions containing 35, 3.5 and 0.035 gm per litre of sodium chloride were also used in some experiments. The conductivity of all the liquid samples was carefully measured both before and after each experimental run, using a standard conductivity measuring bridge possessing a measuring range from 10^{-2} up to 10^{6} μ mho's/cm. All of the storage bottles used to contain the sea water and distilled water were always initially cleaned with detergent, a dilute solution of chromic acid and finally rinsed with distilled water.

CHAPTER 3

THE HEIGHT AND SIZE OF THE DROPLETS FROM BURSTING BUBBLES.

3.1. Introduction.

The generation of jet droplets by bursting air bubbles is influenced by the jet tube diameter, bubble size and the physical properties of the liquid. The system used in these experiments is an air/water interface. The bubbles were generated from a glass capillary orifice as described in Chapter 2. In this chapter, a study is made of the various factors which influence the size and ejection height of the jet droplets produced. The factors which might be expected to influence the droplet size and height of ejection include the following:

(i) type of liquid

(ii) diameter of the air bubble

Both factors are discussed in the following sections.

3.2. The ejection height of the jet droplets.

The size of the bubble is mainly influenced by the diameter of the capillary orifice and to a lesser extent by the applied pressure to the tubing. An initial study was made of the relation between the jet tube diameter and the bubble diameter, as seen in Fig.3.1. The capillary orifice was slanted at a small angle (of the order of 5 - 10 degrees to the horizontal). It can be seen that there is an almost linear increase of bubble size with orifice size. The bubble size was measured by the technique described in Chapter 2 (Section 2). The diameter of the capillary jet orifice was measured by placing the glass tube vertically beneath a normal microscope with a X10 objective lens.

FIG. 3.1
THE RELATION BETWEEN THE JET TUBE DIAMETER AND BUBBLE DIAMETER.

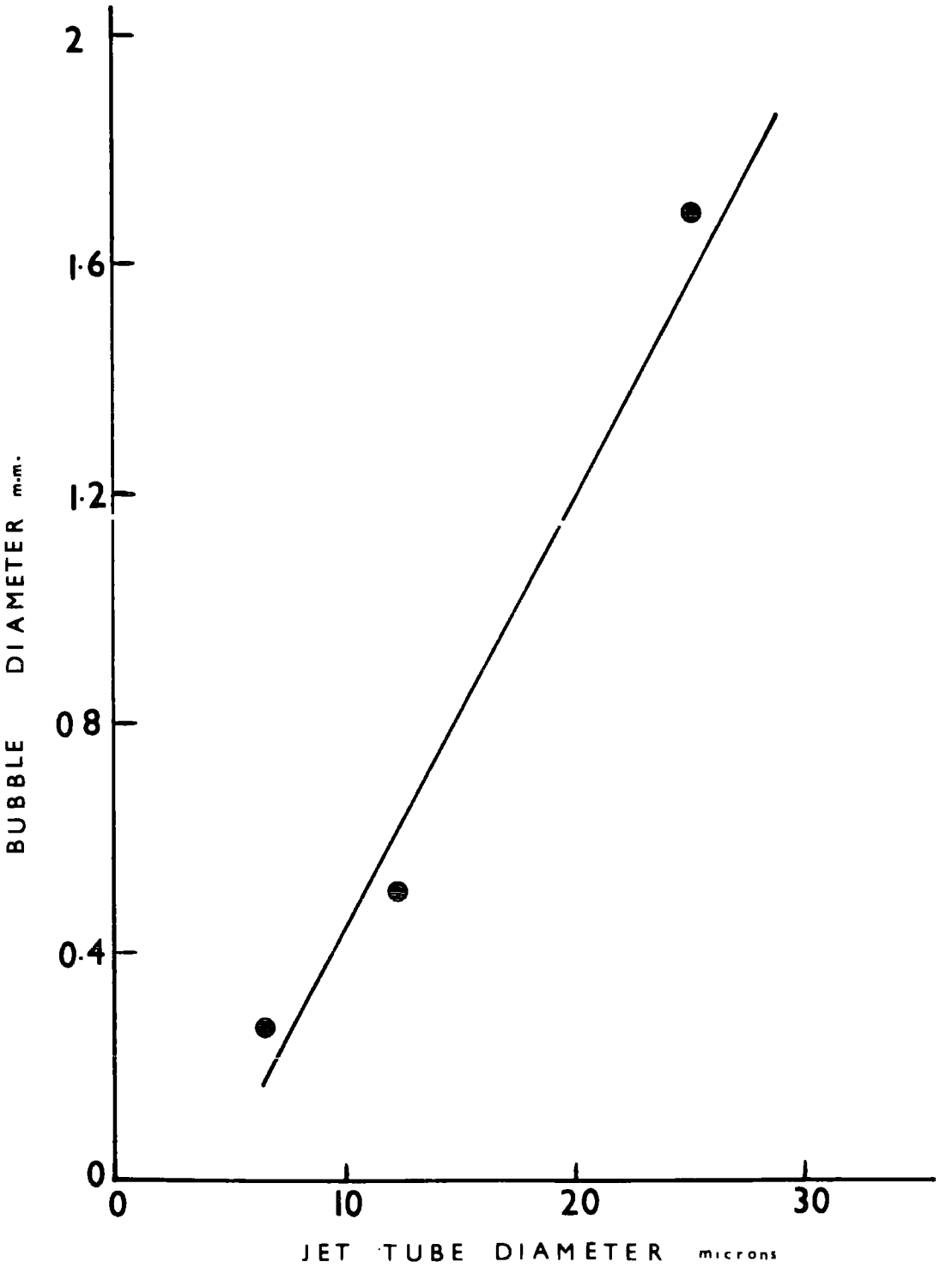

The capillary tubing was placed about 1 to 2 cm beneath the liquid surface in all experiments described in this chapter. The air pressure necessary for bubble production varied from about 1 to 20 psi, depending on capillary tube dimensions. Each bubble breaks at the same point in the liquid surface. In a completely stationery system, the bubbles follow one another along the same path, and if some bubbles rise faster than others, then collision and/or coalescence may follow. This will result in non-homogeneous liquid jet droplet production. However, a slow liquid stream was allowed to continuously create a new liquid surface for efficient bubble bursting.

When a bubble breaks, it ejects four to six jet droplets vertically upwards to various heights. The ejection height of the top droplet from the jet produced from a bursting bubble for deionised water was obtained for bubbles ranging in size from about 0.3 mm to 2.6 mm in diameter, and is shown in Fig.3.2. The shape of the curve agrees closely with results obtained by Stuhlman (1932) who used distilled water for bubble diameters less than about 1 mm. It can be observed that a maximum height of about 12 cm. was obtained for a bubble diameter of approximately 1.1 mm., and falls off to 5 cm. for the largest bubble size of 2.6 mm. The smallest values of ejection height were measured using a travelling microscope, whilst for larger jet droplets the technique outlined in Fig.2.3. was used. A comparison is made in Fig.3.3. between the ejection heights of the top, second, third and fourth droplets respectively for selected bubble sizes. A maximum height value of 2.5cm. was obtained for the second droplet when the bubble diameter was about 0.45 mm. The third and fourth droplets attain maximum ejection heights of approximately 1 cm and 0.3 cm respectively for bubble diameters up to 1 mm. For values of bubble size

FIG. 3.2.
VARIATION OF JET DROPLET EJECTION HEIGHT WITH BUBBLE DIAMETER;
● EXPERIMENTAL POINTS, SOLID LINE : STUHLMAN'S CURVE (1932).

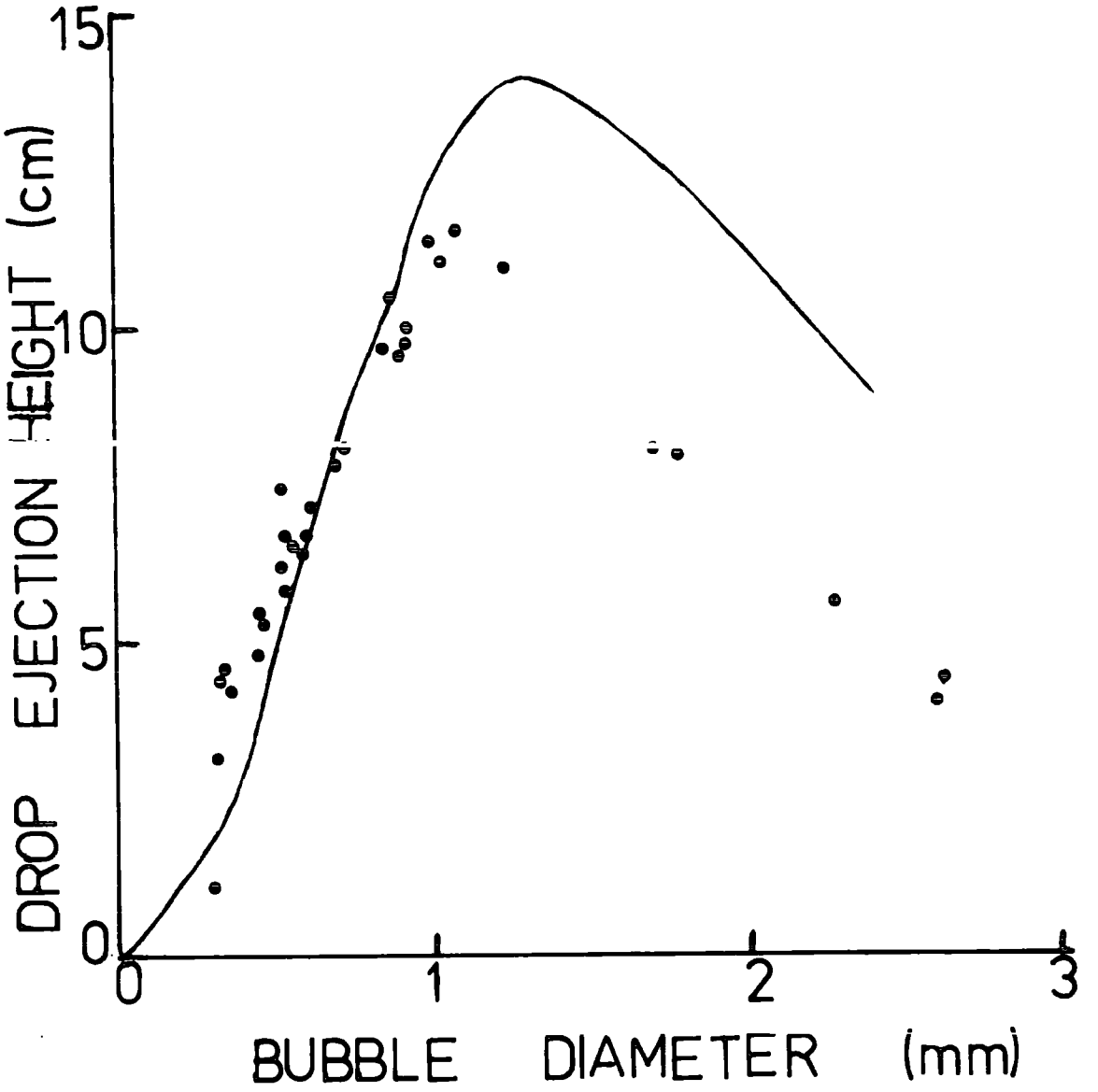

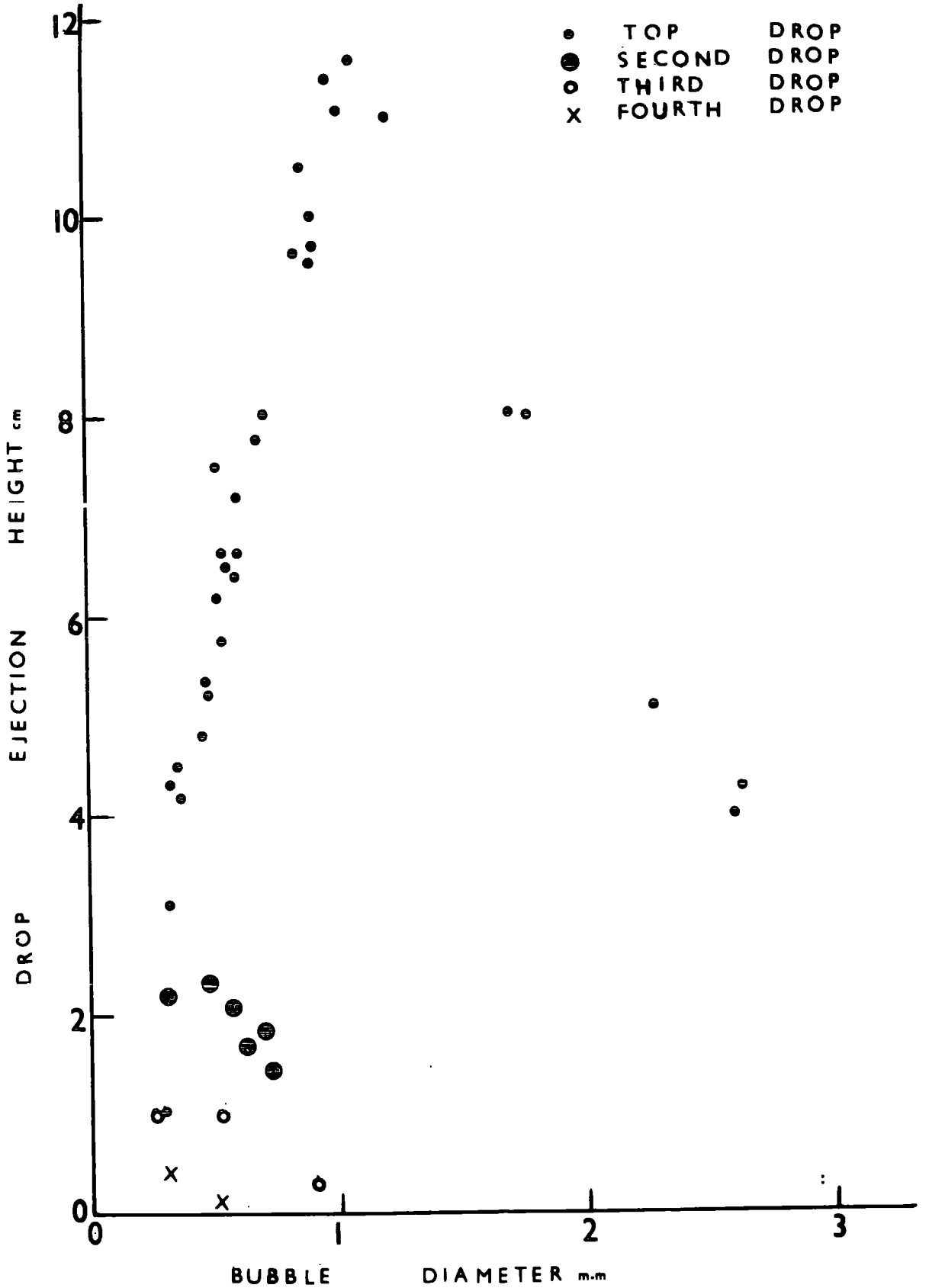

FIG. 3.3.
THE VARIATION OF JET DROPLET EJECTION HEIGHT WITH BUBBLE DIAMETER FOR THE TOP FOUR DROPLETS OF DEIONISED WATER.

in excess of 1 mm it was not feasible to measure droplet ejection heights for droplets other than the top droplet, for deionised water. The results show good agreement with the shape of the curves obtained by Blanchard (1963) for sea-water. Fig.3.4. shows the ejection height of the top droplet for bursting bubbles at a sea-water/air interface. A maximum height of 17.0 cm. was obtained for a bubble diameter of 1.6 mm. It can be noticed that the range of the bubbles is extended to 3.1 mm diameter for sea-water compared to 2.6mm diameter for distilled water for identical capillary jet tubes. In addition, the ejection height is increased. For example, a bubble of diameter 1.6 mm. yields an ejection height of only 9.1 cm for the distilled water compared with 17.0 cm. for sea-water. It may also be seen that for bubble diameters less than 0.84 mm the ejection height of the top jet droplets are identical for both dionised water and sea-water. A comparison between the measurements shown in Figs. 3.2. and 3.4. indicates that for values of bubble diameter greater than about 1.6 mm (bubble size for maximum jet droplet height), there is approximately a constant difference of about 7 cm between the ejection heights of the top droplets.

3.3. <u>The size of the jet droplets</u>

The size of the jet droplets was usually measured by allowing the droplets to impact on to a magnesium coated clean glass slide. The droplet impressions were then measured under a microscope using a specially designed graticule which is described by May (1965). The graticule allowed the droplet impressions to be classified into logarithmically equal intervals each covering a factor of $\sqrt{2}$ in diameter. This greatly facilitated droplet size determination. In general a total of between 10 and 15 droplets were counted from which a

FIG. 3.4.
THE VARIATION OF DROPLET EJECTION HEIGHT WITH BUBBLE DIAMETER FOR SEA WATER.

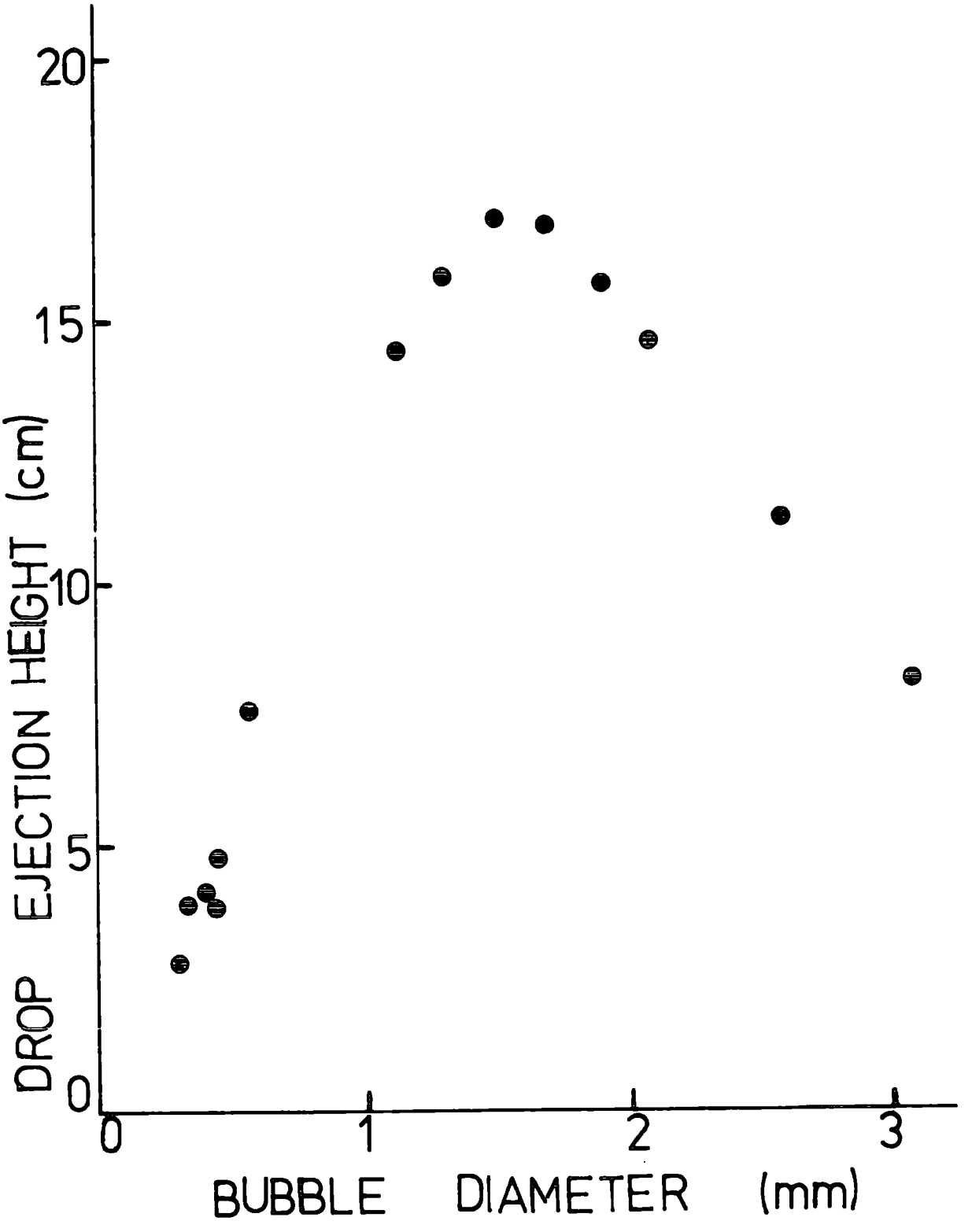

mean droplet size was calculated for each new set of experimental conditions.

A plot of the top jet droplet height as a function of the top droplet diameter is shown in Fig.3.5. for both dionised water and sea-water. As predicted by the results of droplet ejection height versus bubble diameter relation, Fig.3.5. confirms a similar finding in that the jet droplets are ejected to a significantly greater height for droplet diameters in excess of about 200 micrometres for the sea-water medium. The difference in ejection height is probably related to the experimental observation that in deionised water a bubble breaks almost immediately on arrival at the liquid surface, whereas in sea-water the bubble tends to remain at the surface for a considerably longer time. This finding is also confirmed by comparing the results of Stuhlman (1932) for distilled water with those of Blanchard (1963) for sea-water.

The variation of the top jet droplet size with bubble diameter for both distilled water and sea-water is shown in Fig.3.6. The measurements suggest that the droplet size is approximately the same for both distilled water and sea-water. The measurements show that a power law relation of $D_d \propto D_B^{1.22}$ exists, where D_d is the jet droplet diameter, and D_B is the bubble diameter. This compares favourably with the results of Blanchard (1963) who found a power exponent of 1.30.

Since bubbles larger than about 1 mm in diameter constitute a relatively small fraction of the bubble number distribution produced at sea, it can be inferred that the majority of jet droplets produced under natural conditions probably do not exceed about 200 micrometres in diameter. However the bubble production technique proves to be a convenient method for the production of either single or a

FIG. 3.5.
A COMPARISON OF THE JET DROPLET EJECTION HEIGHTS AS A FUNCTION OF JET DROPLET DIAMETER FOR DEIONISED WATER AND SEA WATER.

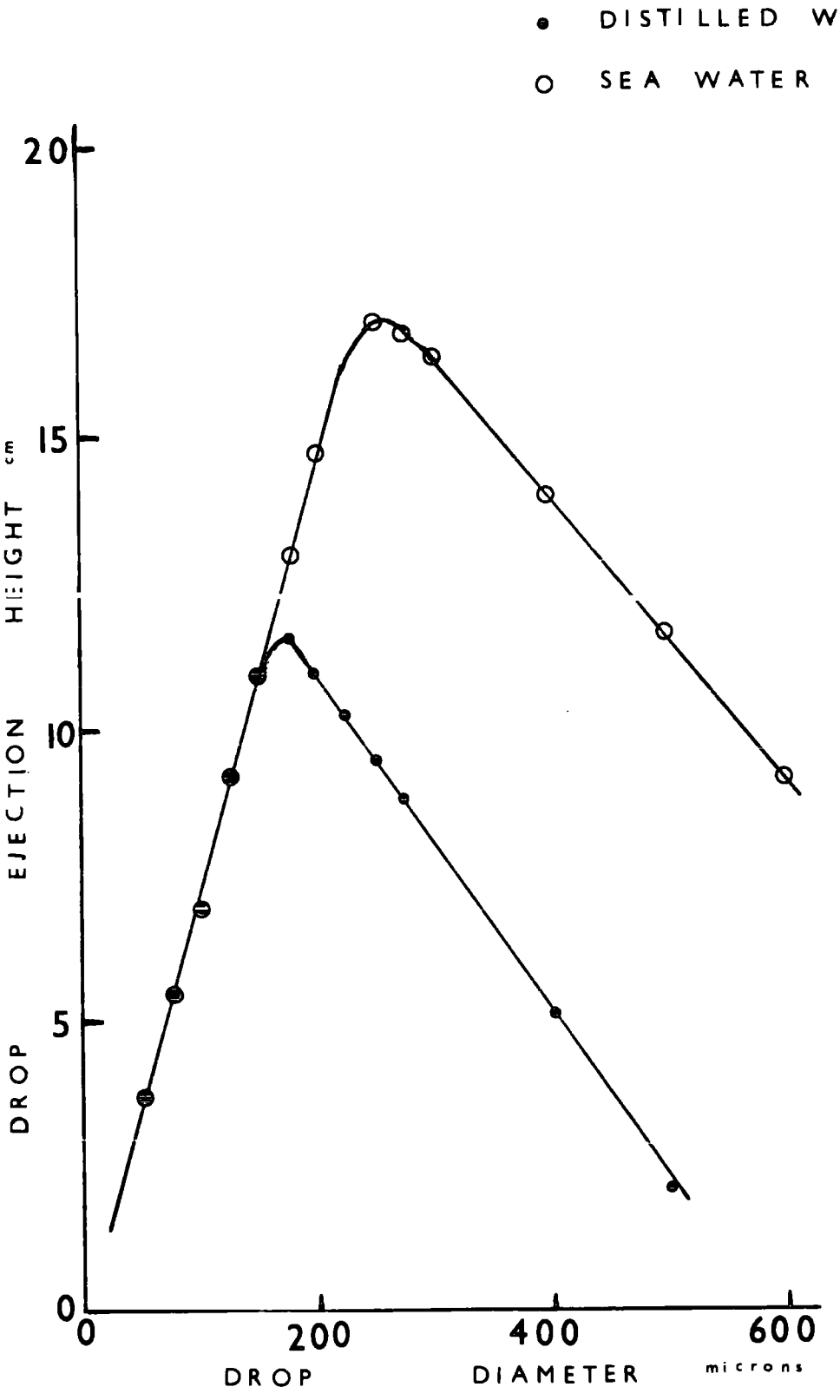

FIG. 3.6.
THE TOP DROPLET SIZE AS A FUNCTION OF BUBBLE DIAMETER FOR DEIONISED WATER AND SEA WATER.

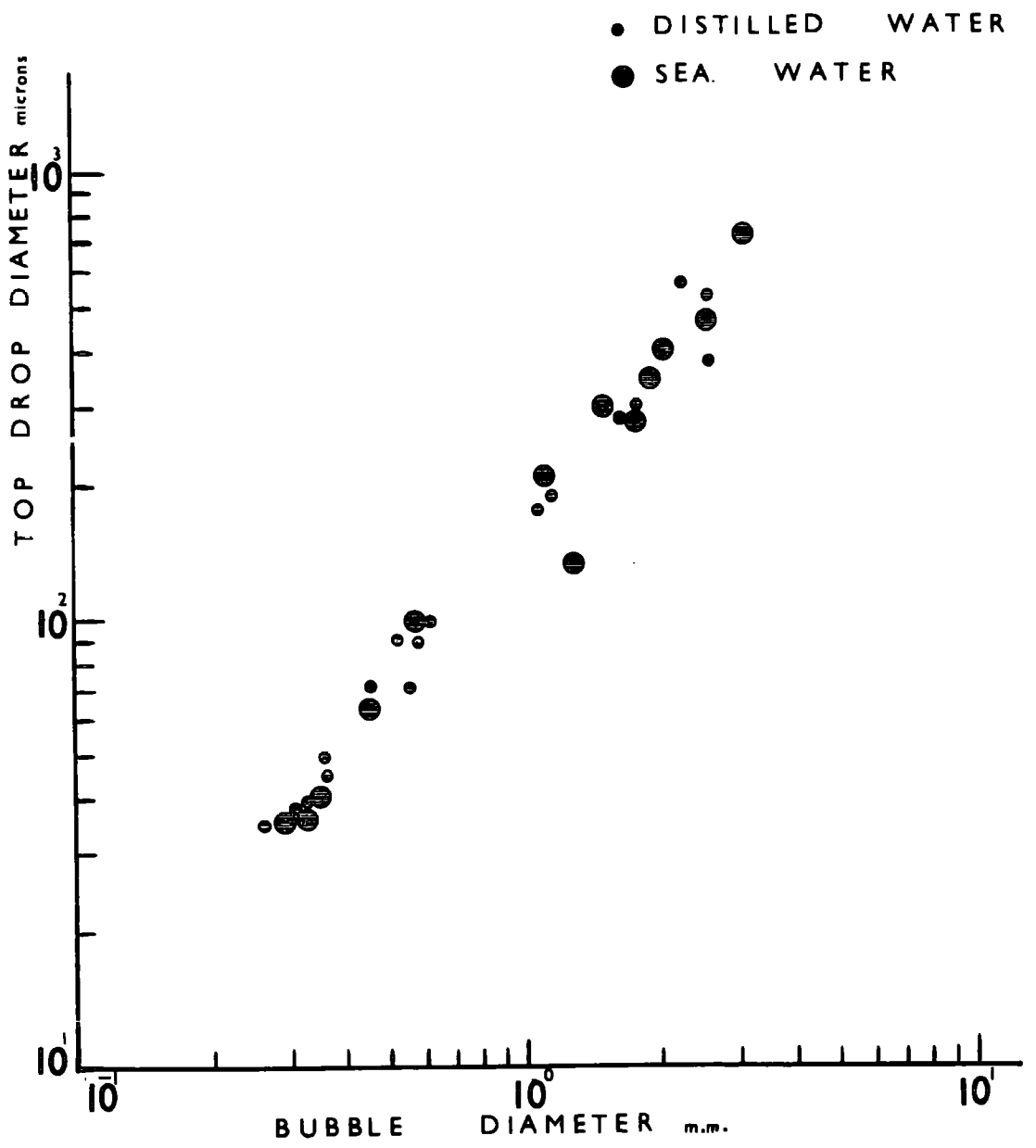

continuous stream of liquid droplets over a wide spectrum of sizes ranging from about 20 to 600 micrometres in diameter. This could be particularly useful for the investigation of drop-collision interaction between liquid droplets of varying size.

The relation between the jet droplet size for the top and second droplet was studied over a wide range of bubble sizes from about 250 up to 900 micrometres in diameter. It can be seen that the second droplet possesses a size of about 60 per cent smaller on average than the top droplet. The percentage difference between the droplet sizes appears to increase for increasing bubble diameter.

FIG. 3.7.
THE VARIATION OF DROPLET DIAMETER WITH BUBBLE DIAMETER FOR THE TOP AND 2ND DROPLET OF DEIONISED WATER.

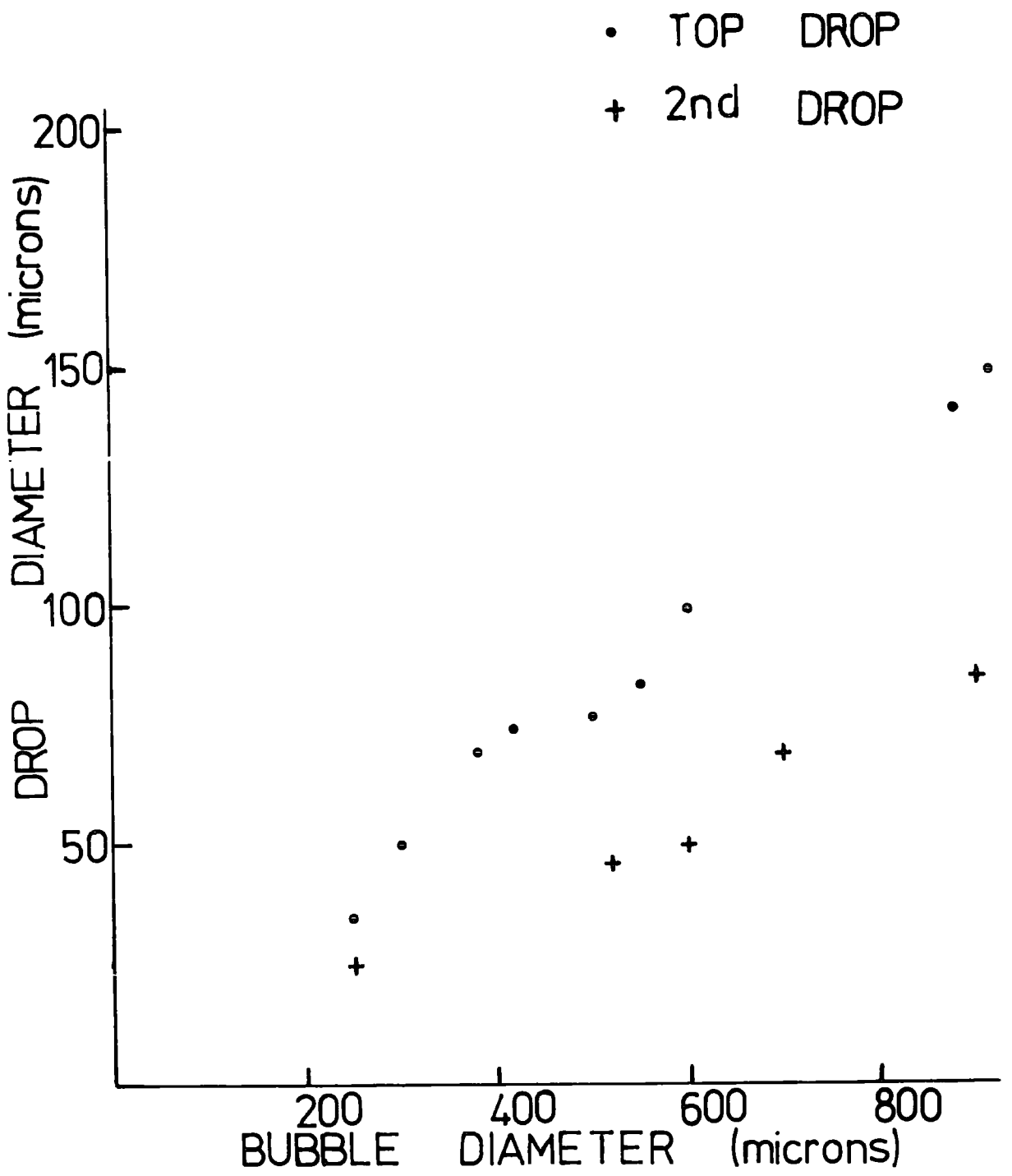

CHAPTER 4.

THE NATURAL AND INDUCTIVE CHARGE OF JET DROPLETS.

4.1. Introduction.

The first report that droplets produced by the vertical jet from a bursting bubble were electrically charged was made by Woodcock et al (1953). Measurement of both the natural and induced electric charge in these droplets was first made by Blanchard (1955, 1958) for sea-water. For a droplet range from about 4 to 26 micrometres in diameter he measured droplet charges from 7×10^{-8} up to about 5×10^{-4} esu respectively, using a Millikan chamber. Blanchard (1963) extended his charge measurements to NaCl solutions. He also studied the effect of bubble age on the magnitude of the charge. Positive charge was only obtained in the experiments. The droplet diameter was extended to about 100 micrometres, whilst little information was obtained for the second droplet in the jet. Some induction charging experiments were also carried out by Blanchard (1963), who used induction fields up to 600 V cm^{-1} for both sea-water and dilute sodium chloride solutions for jet droplets of 17 micrometres in diameter. He found a linear relation between the inductive charge and the applied electric field.

In the present work, studies of the jet droplet natural charge are made over a wider range of droplet size (up to 200 micrimetres in diameter) for sea-water, deionized water, tap water and a wide range of sodium chloride solutions. In addition, results are presented for the second jet droplet. The effect of bubble age on the droplet charging is examined. A series of experiments on the inductive charging for both

small and large (up to $\pm$ 700 V cm^{-1}) values of electric field over a wide range of droplet size is also described.

4.2. Natural charge of the jet droplet as a function of droplet size and bubble age.

The bubble age is defined as the time required to rise from the capillary tip to the liquid surface. The distance between the liquid surface and the capillary tip was measured with a travelling microscope for shorter distances and by a cathetometer for the longer distances. The time was measured by means of a stop watch and repeated trials (usually of the order of 10) gave an accurate estimate of the bubble age. For bubble ages less than about a second, the stop-watch technique was not considered sufficiently accurate and the value was obtained by extrapolation from the curve as in Fig. 4.1. It can be observed that the age of the bubble increases with decreasing size, as is expected. It was also found that the bubble bursts immediately it reaches the liquid surface for both deionized water and low concentrations of sodium chloride solutions, for bubble sizes less than about 2 mm in diameter. However, the bubble has a surface lifetime which increases for increasing bubble diameter, above about 600 micrometres diameter for sea-water and high concentrations of sodium chloride solutions.

The size of the top jet droplet ranged from 18 to 140 micrometres in radius. The Millikan chamber was used for the smaller radius range up to about 65 micrometres, whilst the Faraday cage technique (described in Chapter 2) was used for larger droplets. It was found that all droplets carried a positive charge.

FIG. 4.1.
THE RELATION BETWEEN BUBBLE AGE AND THE DISTANCE BETWEEN THE CAPILLARY TIP AND THE LIQUID SURFACE.

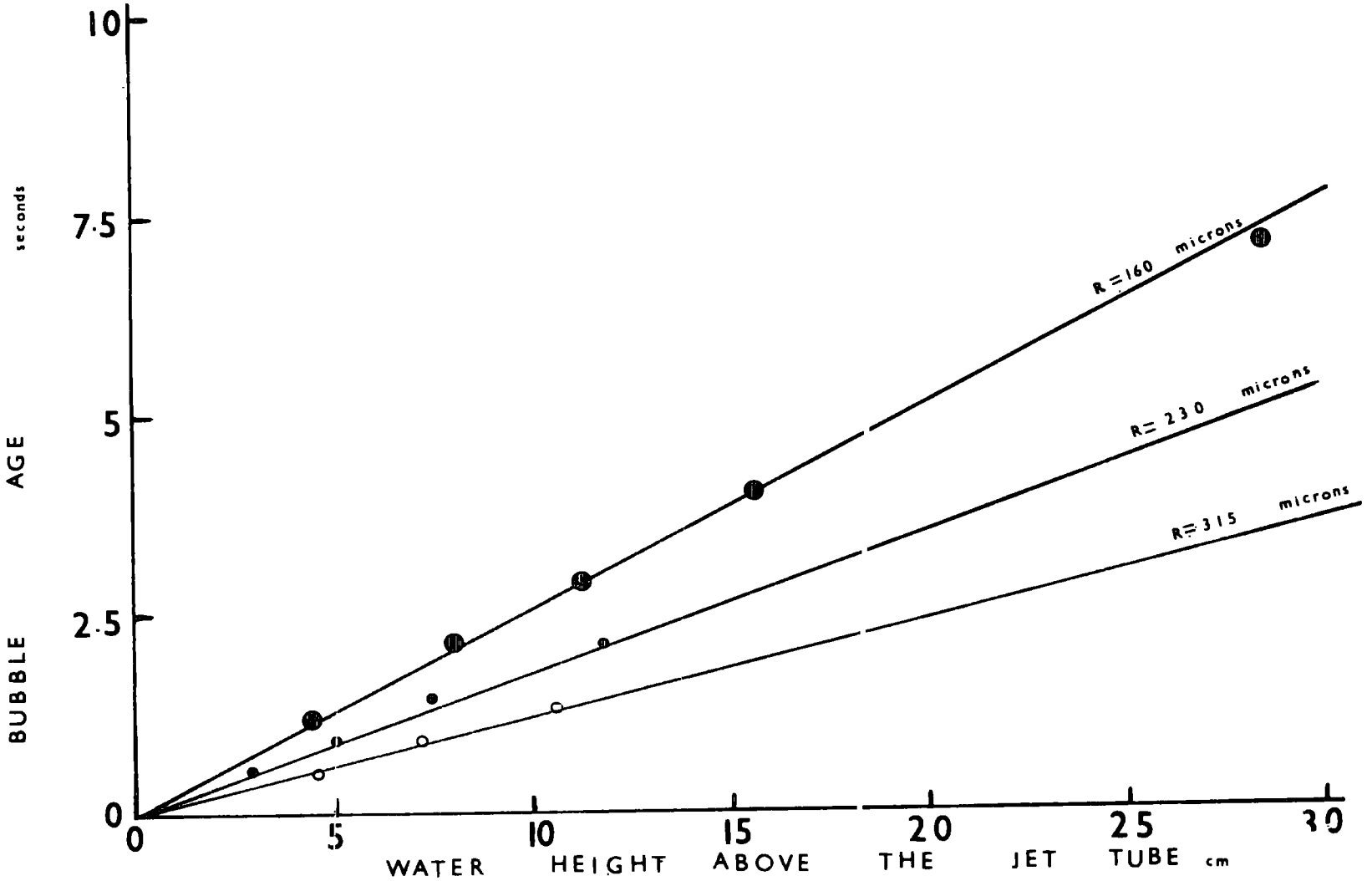

Fig. 4.2. shows the relation between top droplet charge, q, as a function of drop radius for three bubble ages of 0.3, 4 and 6 seconds respectively. The results are for a liquid medium of deionized water which possessed a conductivity of 2.8 μmho's cm^{-1}. All measurements were carried out at room temperature. For the smallest bubble age, the charge increases from about 4×10^{-6} up to 9×10^{-5} esu as the droplet radius is increased from 17 up to 65 micrometres. A plot of these results from Fig. 4.2. on log-log paper indicated that the charge q is related to the droplet size, r, by the expression:

$$q \propto r^{2.4} \qquad (4.1).$$

This predicts a steeper increase in charge than that obtained by Blanchard (1963) who found $q \propto r^{1.3}$ for the much narrower size range of 5 to 20 micrometres. It can be seen from Fig. 4.2. that the charge increases with increasing bubble age as also observed by Blanchard.

Natural charge measurements were carried out for sea-water for bubble ages of 0.3 and 6 seconds and are plotted against jet droplet radius in Fig. 4.3. The conductivity of the sea-water was 4.1×10^{4} μmho's cm^{-1}. A comparison of Fig. 4.3. with Fig. 4.2. shows that over the jet droplet radius range from about 19 to 30 micrometres, the droplet charge is about a factor of between 5 and 6 greater for deionized water than for sea-water, for the bubble age of 0.3 seconds. The increase in charge for the larger bubble age of 6 seconds is about 50 and 30 per cent for droplet radii of 19 and 30 micrometres respectively.

It was not possible to investigate the relation between charge and droplet radius beyond 30 micrometres, since the bubbles did not burst in a regular manner for greater bubble

FIG. 4.2.
THE TOP JET DROPLET CHARGE AS A FUNCTION OF DROPLET SIZE AND BUBBLE AGE FOR DEIONISED WATER.

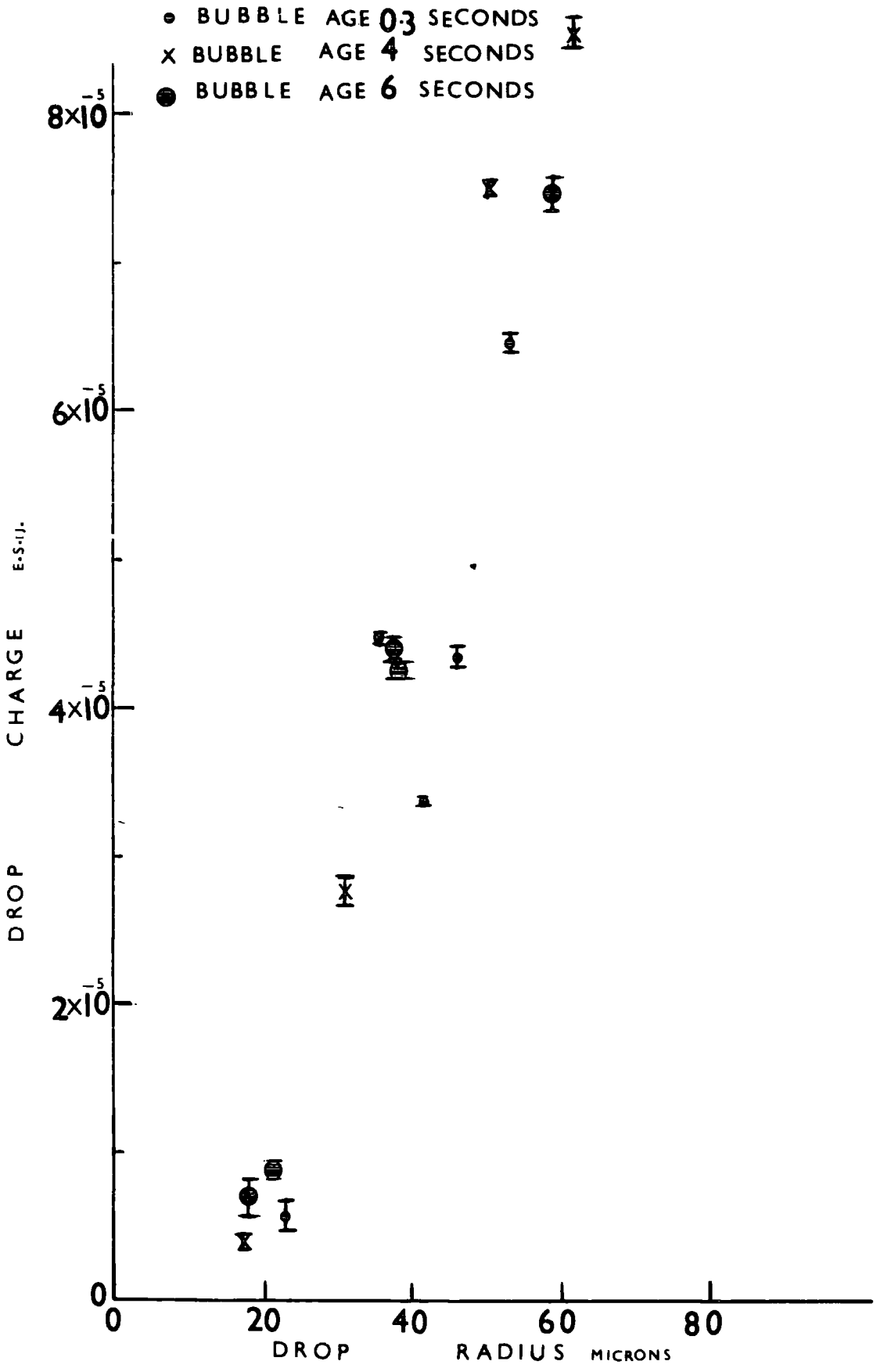

FIG. 4.3.
THE RELATION BETWEEN THE TOP JET DROPLET CHARGE AND DROPLET RADIUS FOR BUBBLE AGES OF 0.3 AND 6 SECONDS, FOR SEA WATER.

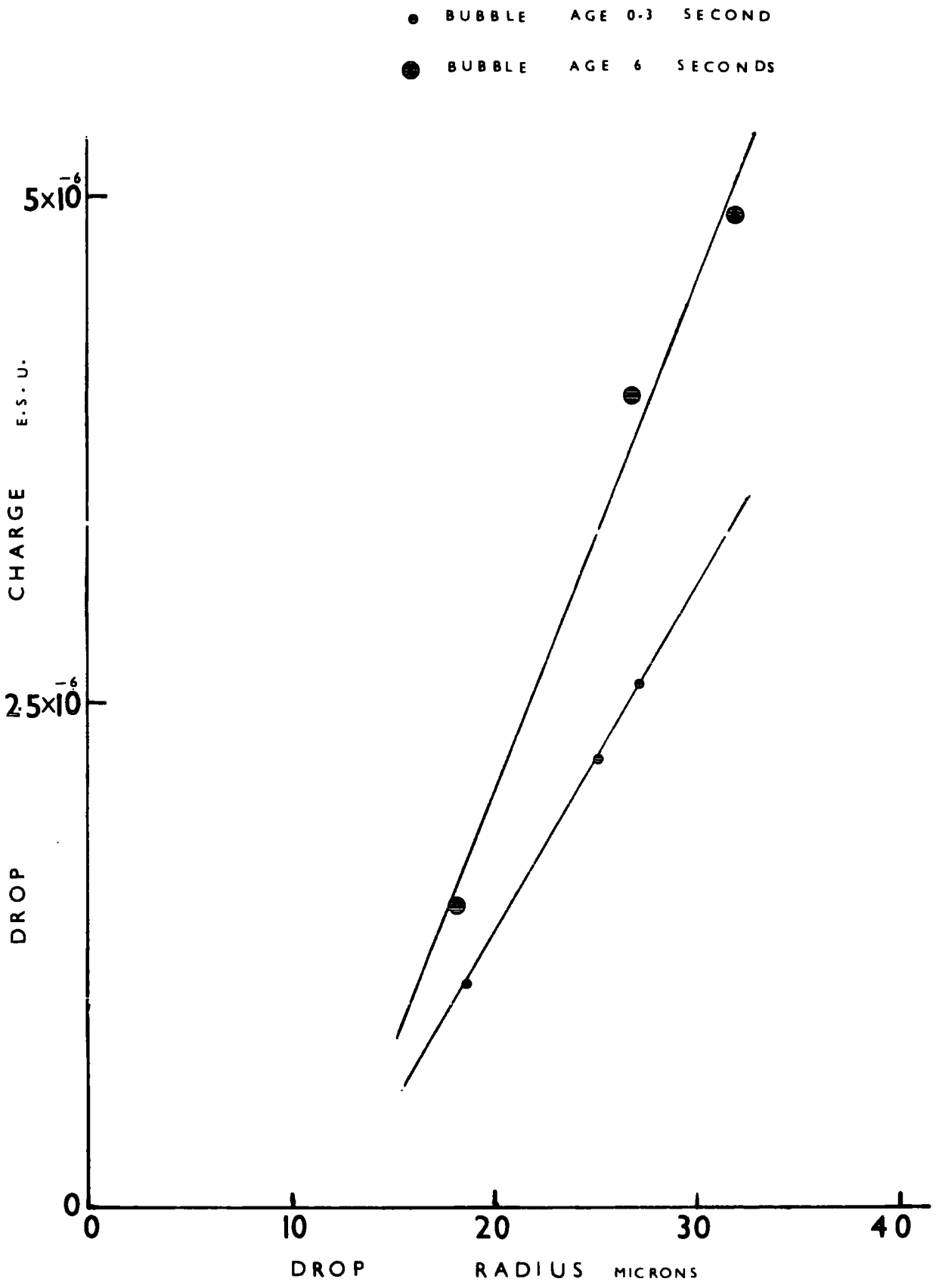

sizes. This was due to coalescence between bubbles which were remaining on the liquid surface and rising bubbles from the capillary tip. This resulting coalescence gave rise to droplets of varying size which impeded accurate measurement of the charge/size relation.

A number of experiments were carried out on the second jet droplet and the measurements of electric charge with droplet size were shown in Fig. 4.4. for bubbles bursting in deionized water. There was a greater fluctuation observed for the investigations carried out on bubble age. A comparison between the top and second droplet shows that the natural charge on the second droplet varies from about 100 per cent to about 25 per cent of the top droplet charge over the range of droplet size as seen in Fig. 4.5. As before, the polarity of charge for the second jet droplet was found to be positive. The bubble age was 0.3 second (capillary tip about 2 cm below the water surface) for the above comparison.

4.3. Natural charge on jet droplets greater than 60 micrometres in radius.

In order to extend the range of electric charge for droplets greater than about 60 micrometres in radius a technique other than a Millikan chamber was necessary. A method employing a Faraday cage was used and a schematic diagram of the apparatus is shown in Fig. 2.6. A comparison was first made between measured charges using a Millikan chamber and the Faraday cage system, for the bubble ages of 0.3 and 3.5 seconds. Deionized water was used for this comparison and the results are shown in Table 4.1. The tabulated values were obtained by extrapolation from Figs. 4.2. and 4.6. for the bubble age of 0.3 seconds. Actual measured values were used in compiling the data for the bubble age of 3.5

FIG. 4.4.
THE VARIATION OF CHARGE WITH DROPLET RADIUS FOR BUBBLE AGES 0.3 AND 3.5 SECONDS, FOR THE SECOND JET DROPLET OF DEIONISED WATER.

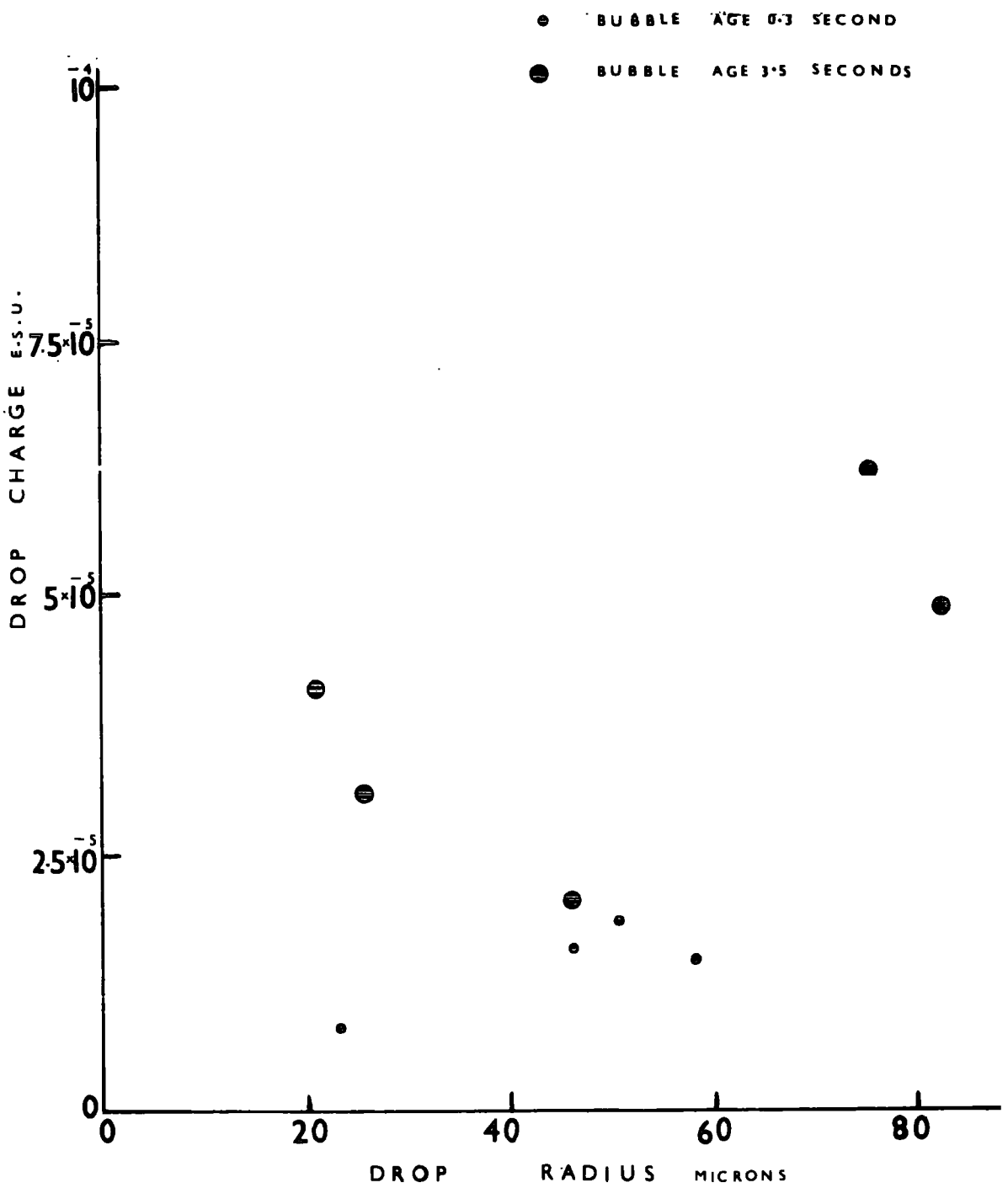

FIG. 4.5.
A COMPARISON BETWEEN THE CHARGE OF THE TOP AND SECOND JET DROPLET AS A FUNCTION OF SIZE.

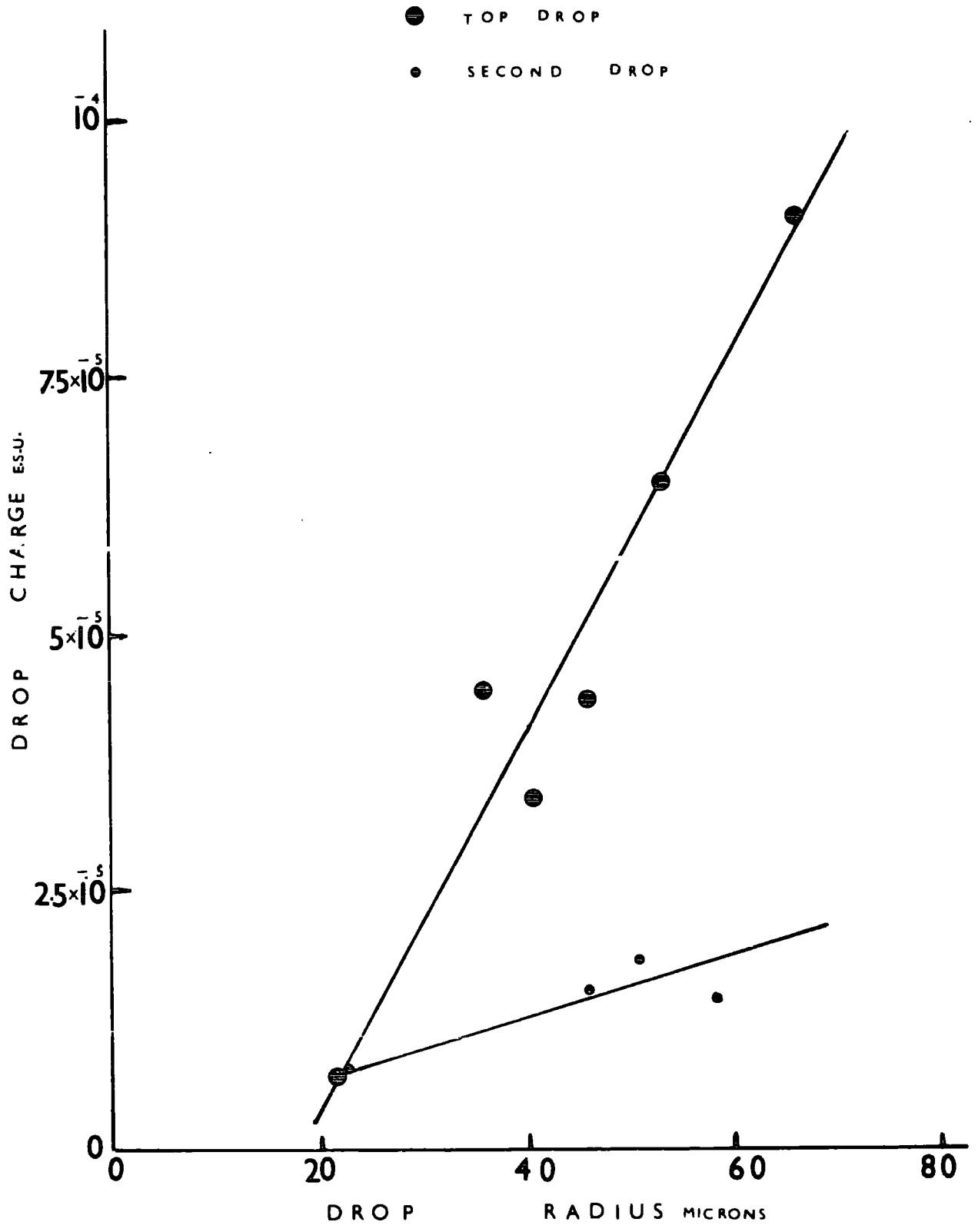

TABLE 4.1.

BUBBLE AGE: (sec).	DROPLET RADIUS: (micrometres).	DROPLET CHARGE USING A MILLIKAN CHAMBER. x 10^{-6} esu.	DROPLET CHARGE USING A FARADAY CAGE. x 10^{-6} esu.
0.3	25	4.5	4.5
	30	22.6	17.5
	40	41.2	31.0
	50	59.8	44.3
	60	78.0	57.5
	70	No suspension.	39.5
3.5	25	17.5	17.6
	35	36.0	37.2
	70	No suspension.	41.0

seconds. Agreement between the experimental values of droplet charge is reasonably good for values of droplet radius less than 35 micrometres. However, the droplet charge using the Millikan chamber was 35% larger on average than that obtained by the Faraday cage method for larger jet droplets. This may be partly attributed to the addition of an inductive charge (positive) to the natural charge on the droplets from the field lines of the suspension field of the Millikan chamber.

A study of the natural charge of the top jet droplet ranging in radius from 25 up to 142 micrometres was made using the Faraday cage and the results are shown in Fig. 4.6. It shows a peak in the top droplet charge at around 6.0×10^{-5} esu, thereafter decreasing to values of approximately 3×10^{-6} esu for droplet radii of 100 micrometres and greater. It was not possible to reliably use the Faraday cage to measure the charge for droplets of radius greater than about 145 micrometres. This is because the bubbles did not burst in a reproducible constant manner at the water surface for bubble size greater than about 900 micrometres in radius. Constant droplet production was a necessary pre-requisite for accurate charge measurement using the Faraday cage system. The falling off of electric charge with increasing droplet size is a novel result in jet droplet charging work. A study of droplet charging for droplets greater than about 20 micrometres in radius has not previously been undertaken. A further discussion of these results will be presented in Chapter 5.

The relation between top droplet charge and bubble age is illustrated in Fig. 4.7. for a range of droplet radii from 20 up to 71 micrometres. With the exception of the experimented points for a droplet radius of 36 micrometres, where tap-water

FIG. 4.6.
THE RELATION BETWEEN TOP DROPLET CHARGE AND SIZE FOR BUBBLE AGES 0.3 AND 3.5 SECONDS OVER A LARGER DROPLET SIZE RANGE.

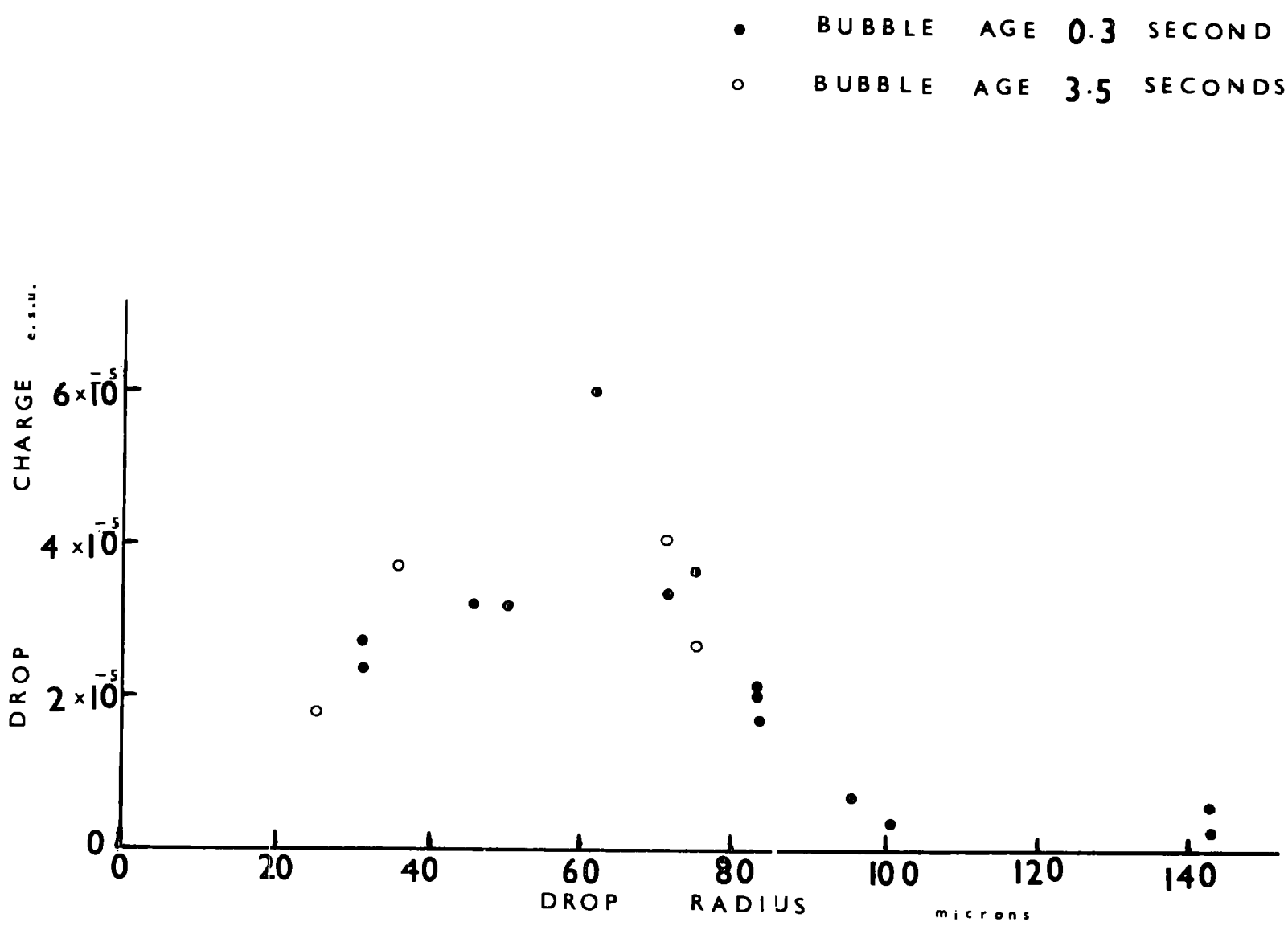

FIG. 4.7.
THE CHANGE IN TOP JET DROPLET CHARGE WITH BUBBLE AGE FOR A RANGE OF DROPLET SIZES.

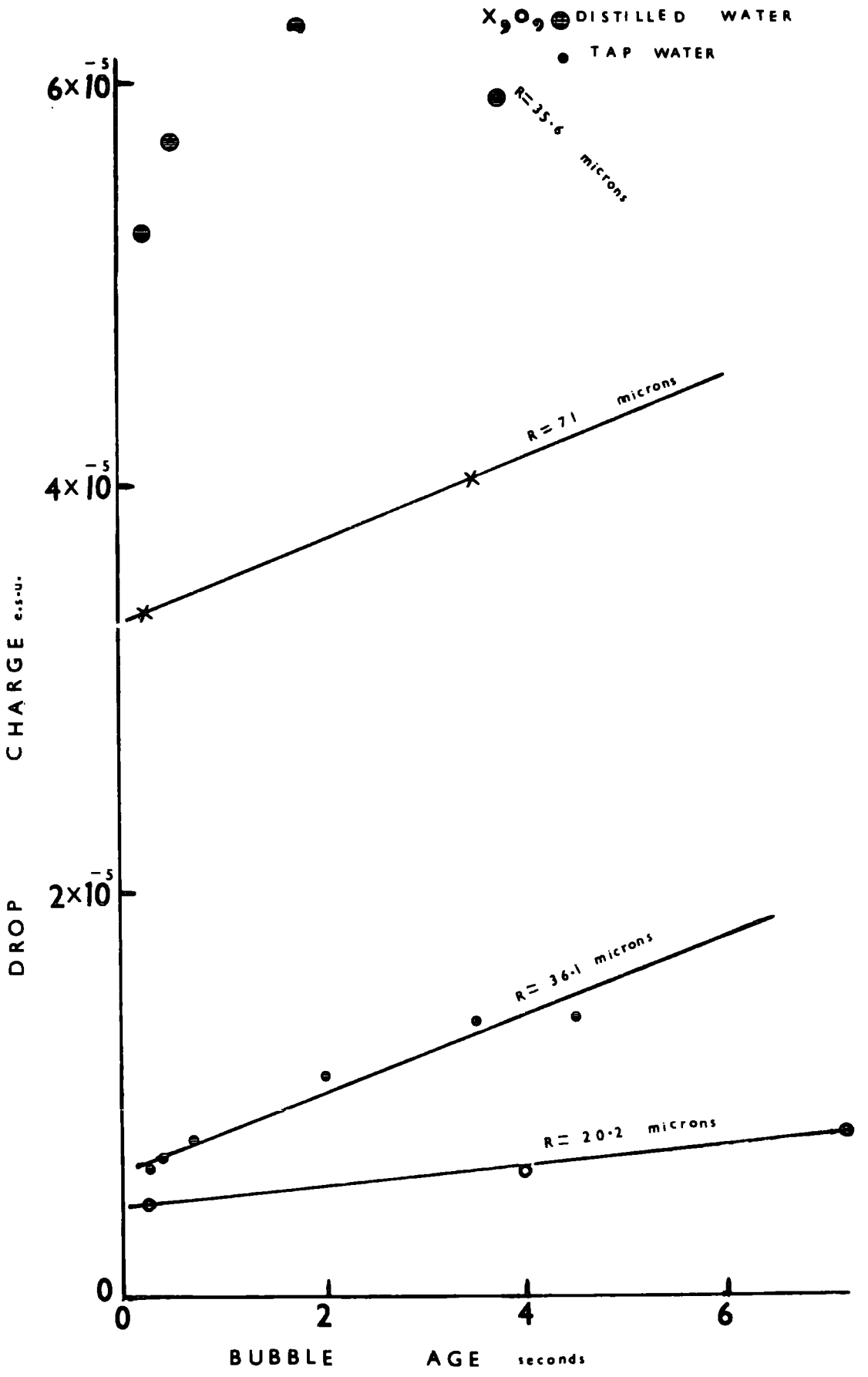

was used, distilled water was used throughout. The results suggest that the electric charge is a slow increasing function of bubble age. A log-log plot for the most numerous experimental points for tap-water (droplet radius R = 36.1 micrometres) indicates a straight line with a charge, q, versus bubble age, t, relation of $q \propto t^{0.28}$. This compares favourably with the relation $q \propto t^{0.4}$ obtained by Blanchard (1963) for the smaller droplet radius range from about 4 to 20 micrometres for sea-water. In addition, it can also be seen that the top droplet charge for deionized water for a droplet radius of 36 micrometres is a factor of from 5 to 6 greater than that for tap-water over the range of bubble age. This result is similar to that found for sea-water.

4.4. Natural charge as a function of water conductivity and bubble age.

Several types of water were used in this investigation ranging from deionized water of conductivity 2.8 μmho's cm^{-1} up to 4×10^4 μmho's cm^{-1} for sea-water. In addition, salt solutions of varying concentration from 2×10^{-4} gm per litre up to 35 gm per litre which yield conductivities from 2.9 up to 4×10^4 μmho's cm^{-1} respectively. A salt concentration of 35 gm per litre (or 0.6 M of sodium chloride) was chosen since it corresponds to the same salinity as sea-water of 35,000 ppm. A measured relation between salt concentration and water conductivity as measured by a standard conductivity cell is shown in Fig. 4.8., which shows a reasonably good linear relation as expected.

The relation between top droplet charge and bubble age for distilled water, sea-water and three salt solution concentrations of 0.035, 3.5 and 35 gm per litre is shown in

FIG. 4.8.
THE RELATION BETWEEN SODIUM CHLORIDE CONCENTRATION AND WATER CONDUCTIVITY.

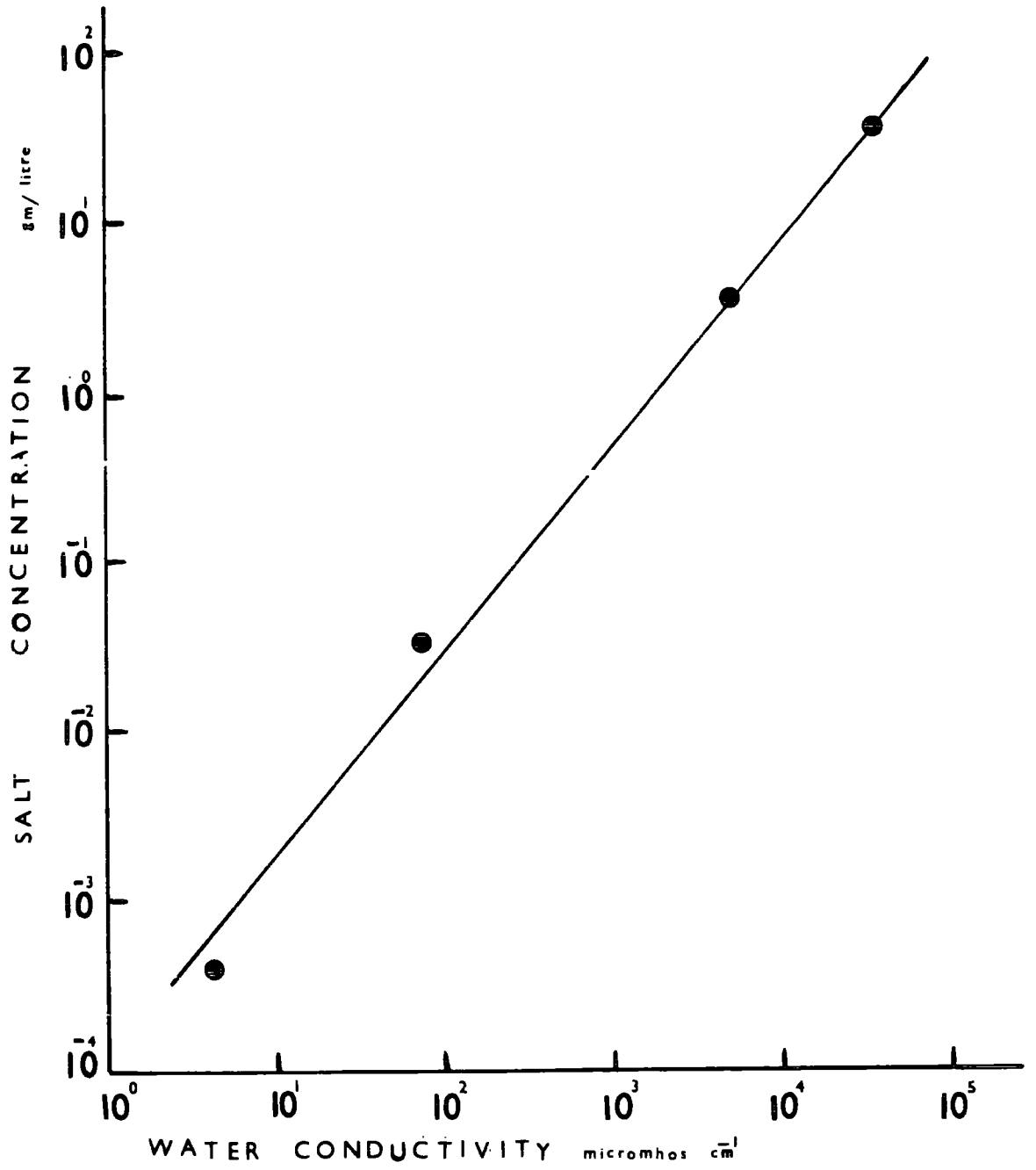

Fig.4.9. Each curve is labelled by the jet droplet radius and shows a slow increase of charge with bubble age. The individual measurements are shown in Table 4.2. The results infer that on average there is a 40 and 80 per cent increase in droplet charge for the more dilute salt solutions ($\leq$ 3.5 gm per litre) as the bubble age increases from 0.25 to 4 seconds and 7 seconds respectively. For the artificial sea-water and sea-water, an average increase of 25 per cent in droplet charge is obtained for an increase in bubble age from 0.3 to 7 seconds.

The variation of the top droplet charge with water conductivity is shown in Fig.4.10 for the three bubble ages of 0.3, 4.0 and 7.0 seconds. The curves show that the charge increases by about a factor of 3 for all bubble ages considered as the conductivity is decreased by about 4 orders of magnitude from the more highly concentrated liquids. A comparison between these results and a charging theory proposed by Iribarne and Klemes (1974) is deferred to Chapter 5 of this thesis. It can also be seen from Fig.4.10 that the effect of bubble age is greatest for the more dilute solutions, and that there is a greater rate of increase of droplet charge with decrease in conductivity for the larger bubble ages.

4.5. Inductive charging of jet droplets.

The measurement of induction charge on the jet droplets was made by the Millikan chamber and the Faraday cage system as shown in Figs. 2.7(a) and (b). The electrostatic shielding screeen was removed from beneath the Millikan chamber and the Faraday cylinder for these studies. The effect of bubble age makes no difference to the inductive charge as predicted.

FIG. 4.9.
THE CHARGE OF THE TOP JET DROPLET AS A FUNCTION OF BUBBLE AGE FOR DIFFERENT LIQUID MEDIA.

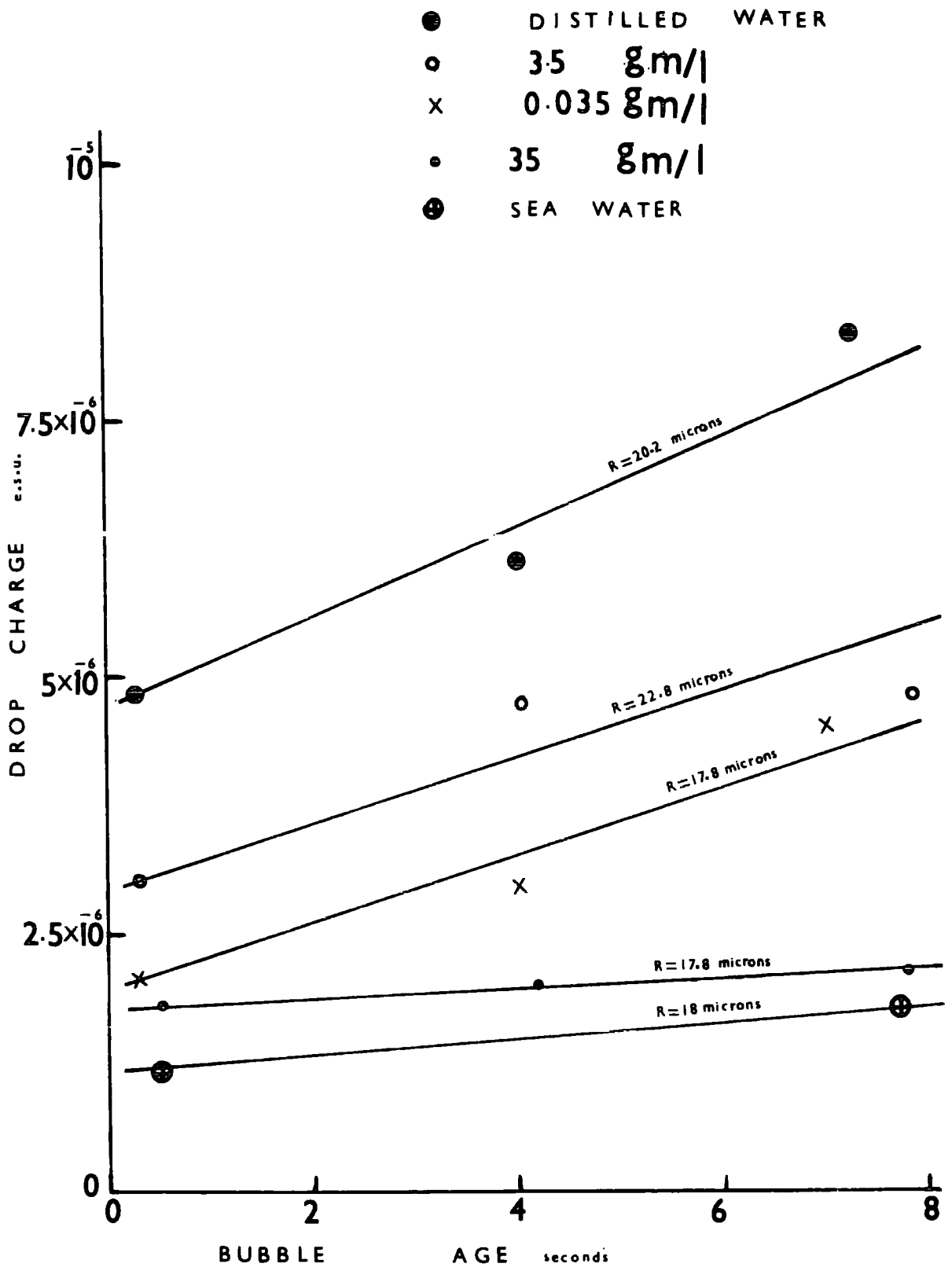

FIG. 4.10.
THE RELATION BETWEEN DROPLET CHARGE AND WATER CONDUCTIVITY FOR BUBBLE AGES OF 0.3, 4 AND 7 SECONDS.

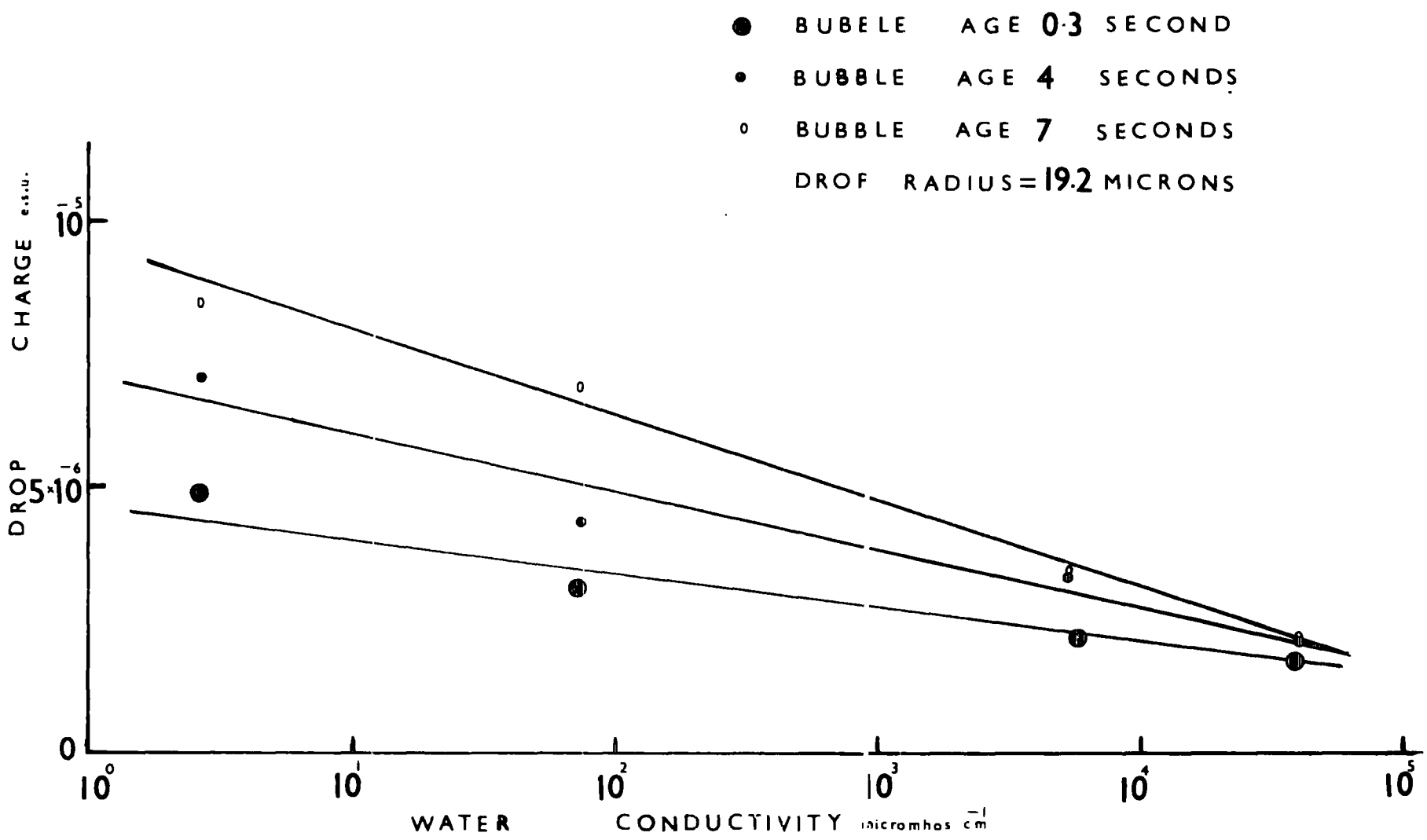

TABLE 4.2.

BUBBLE DIAMETER: (Micrometres)	TOP DROPLET RADIUS: (Micrometres)	BUBBLE AGE: (Seconds)	TYPE OF WATER:	SALT CONCENTRATION: gm/litre.	WATER CONDUCTIVITY: (μmho's cm^{-1}).	TOP DROPLET CHARGE: (esu).
0.319	20.2	0.25	Deionised	-	2.85	4.95×10^{-6}
"	20.2	4.0	"	-	2.85	6.04×10^{-6}
"	20.2	7.0	"	-	2.85	8.47×10^{-6}
0.319	17.8	0.3	Sodium	0.035	72.5	2.04×10^{-6}
"	17.8	4.0	Chloride	0.035	72.5	2.91×10^{-6}
"	17.8	7.2	Solution	0.035	72.5	4.65×10^{-6}
0.342	22.8	0.3	"	3.5	5.4×10^{3}	3.04×10^{-6}
"	22.8	4.0	"	3.5	5.4×10^{3}	4.84×10^{-6}
"	22.8	7.0	"	3.5	5.4×10^{3}	4.84×10^{-6}
0.335	17.8	0.25	Artificial	35	4×10^{4}	1.80×10^{-6}
"	17.8	4.0	Sea-water	35	4×10^{4}	2.07×10^{-6}
"	17.8	7.0	"	35	4×10^{4}	2.12×10^{-6}
0.30	18.3	0.3	Sea-water	-	4.1×10^{4}	1.1×10^{-6}
"	18.3	7.0	"	-	4.1×10^{4}	1.5×10^{-6}

The experiments were carried out for two ranges of induction voltage, namely a low range of between $\pm$ 10V cm^{-1} and the larger range of $\pm$ 175 V cm^{-1}. The charge for the top jet droplets of radii 46.0 and 35.6 micrometres respectively is plotted as a function of induction field which was varied between $\pm$ 10 V cm^{-1}. An experimental run for the second jet droplet of radius 50 .4 micrometres is also shown. All three curves demonstrate that there is a linear relation between the droplet charge and induction field. Deionized water was used in these experiments. It can also be seen that there is a large reduction (a factor of between 5 and 6) between the charge of the top droplet of radius 46.0 micrometres and the second droplet of radius 50.4 micrometres. This agrees approximately with the previous finding when studying the natural charge on similarly sized droplets as seen in Fig.4.5. It should be noted that the slopes of the three lines drawn in Fig.4.11 are approximately the same.

A linear relation between top droplet inductive charge and the induction field is also obtained for both distilled water and sea-water for the larger range of induction field (maximum is equal to $\pm$ 175 V cm^{-1}). It can be seen that an induction electric field of 90 V cm^{-1} is necessary to neutralize the jet droplet of radius 35.6 micrometres. A much lesser potential difference of 12.5 V cm^{-1} is required to change the polarity of the positive charge of the jet droplet of sea-water.

The range of the inductive field was extended to $\pm$ 700 V cm^{-1}, and inductive charging experiments for the second jet droplet of radius 50 micrometres from distilled water showed that linearity between charge and inductive field was preserved for values of inductive field approaching about 450 V cm^{-1}, as

FIG. 4.11.
THE INDUCTIVE CHARGE OF THE TOP AND SECOND JET DROPLETS FOR VALUES OF INDUCTION FIELD BETWEEN ± 10 V cm^{-1}.

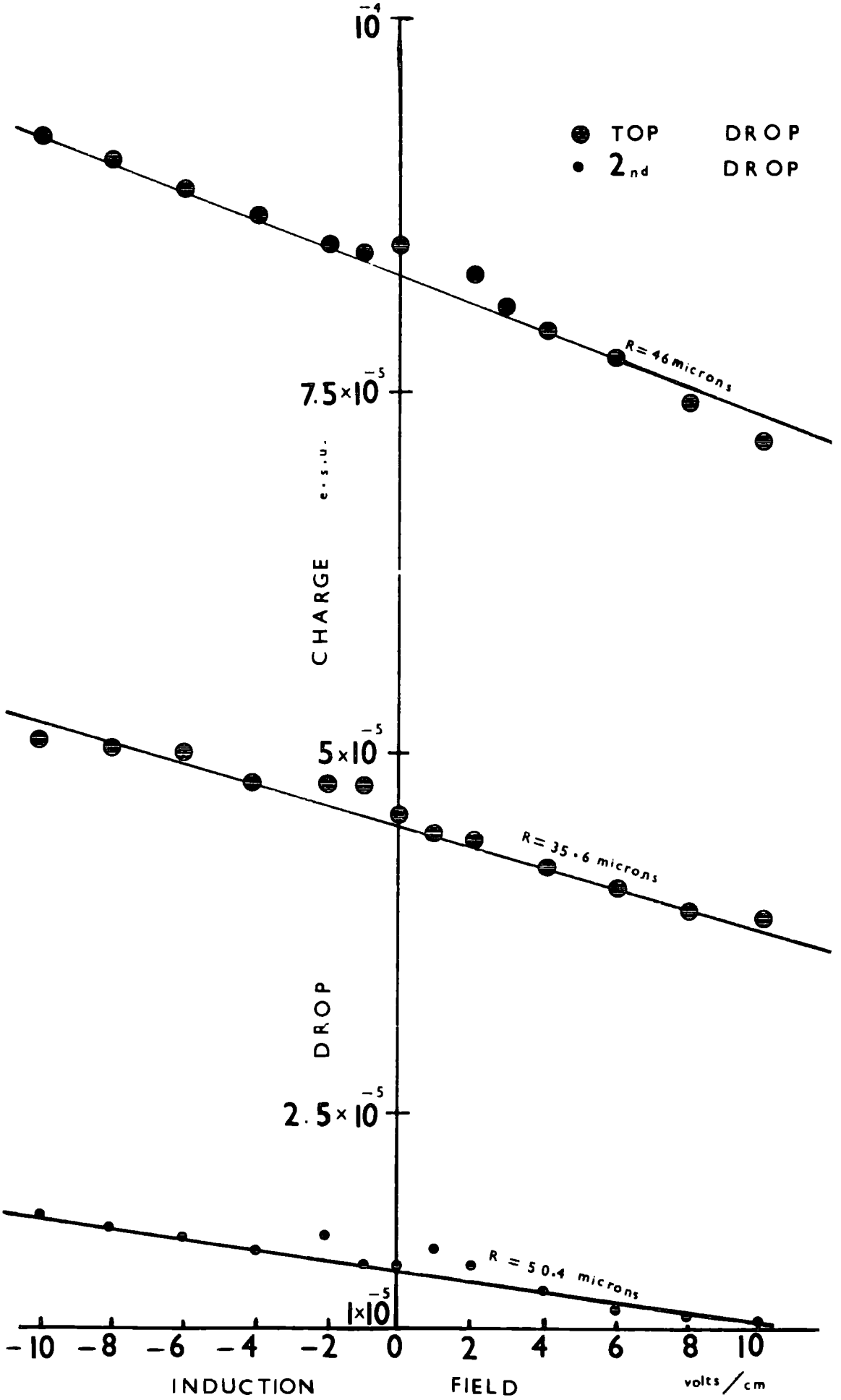

FIG. 4.12.
THE INDUCTIVE CHARGE OF THE TOP JET DROPLET AS A FUNCTION OF INDUCTION FIELD VARIED BETWEEN 0 AND + 175 V cm^{-1} FOR DISTILLED WATER AND SEA WATER DROPLETS.

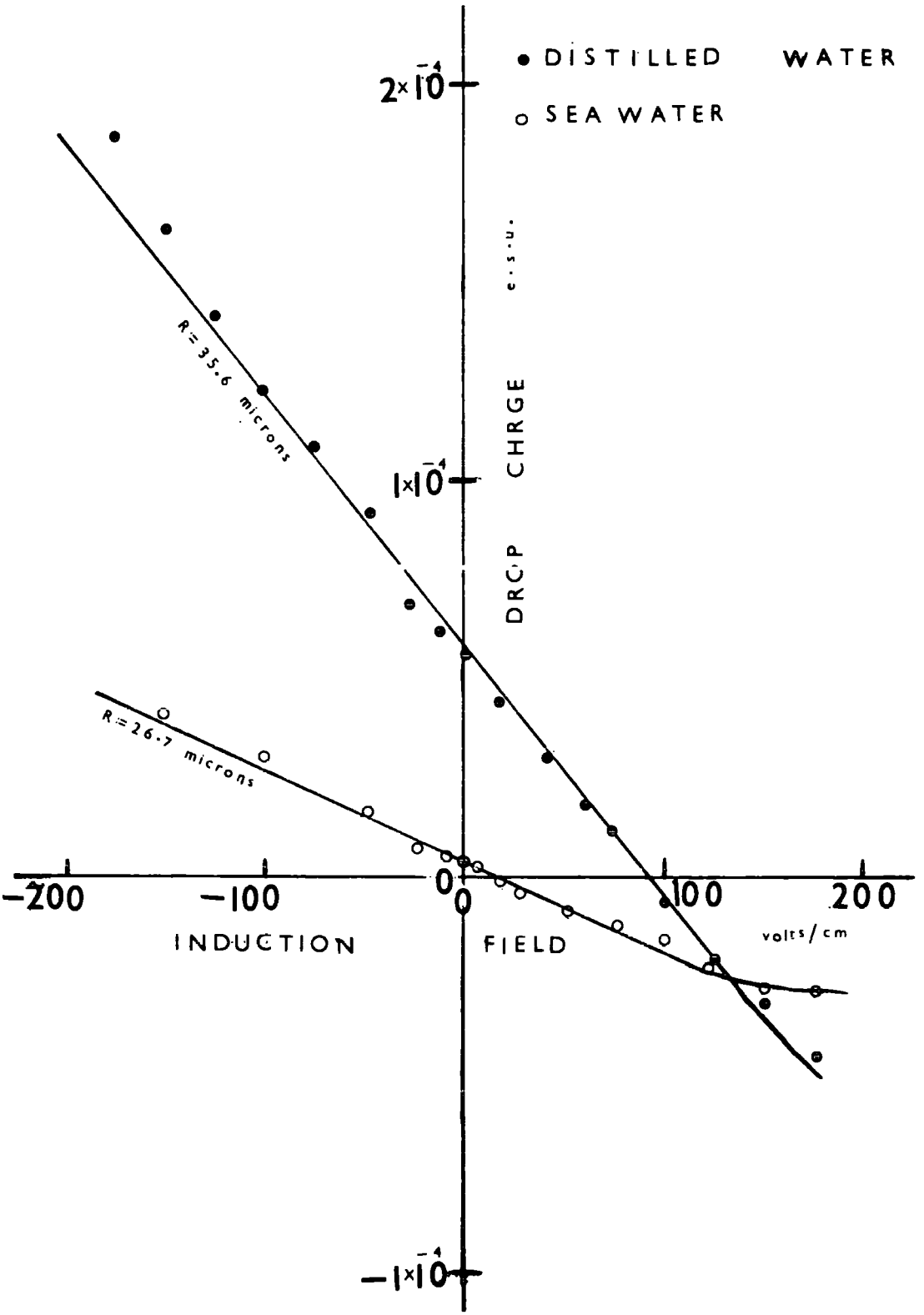

seen in Fig. 4.13. For larger values of inductive field, the inductive charge becomes approximately constant. This may be due to the limitation of the charge by the initiation of corona discharge from the surface of the droplet.

For larger top droplets of distilled water of 75.6 micrometres, the Faraday cage apparatus was used here. The results, shown in Fig. 4.14 give linearity with the low values of inductive field used (0 to $\pm$ 10 V cm^{-1}). It can be observed that a relatively small field of about 8 V cm^{-1} is sufficient to neutralize the charge on the jet droplet. This linearity, with similar slope is maintained for the larger induction fields up to $\pm$ 90 V cm^{-1} as shown in Fig. 4.15 for the same size jet droplets. Distilled water was used as the liquid medium for the last two sets of measurements.

A plot of the inductive charge on the top jet droplet of radius 26.7 micrometres as the induction field is varied between 0 and $\pm$ 25 V cm^{-1} for sea-water is shown in Fig. 4.16. A slight discontinuity in the slope of the experimental points occurs at the transition between positive and negative polarity of charge. An electric field of approximately 12 V cm^{-1} is necessary to change the charge polarity which is in general agreement with preliminary work of Blanchard (1958). A further discussion of these results is presented in the following chapter.

FIG. 4.13.
THE INDUCTIVE CHARGING FOR THE SECOND JET DROPLET FROM DISTILLED WATER OF RADIUS 50 MICROMETRES FOR AN INDUCTIVE FIELD RANGING FROM 0 TO $\pm$ 700 V cm^{-1}.

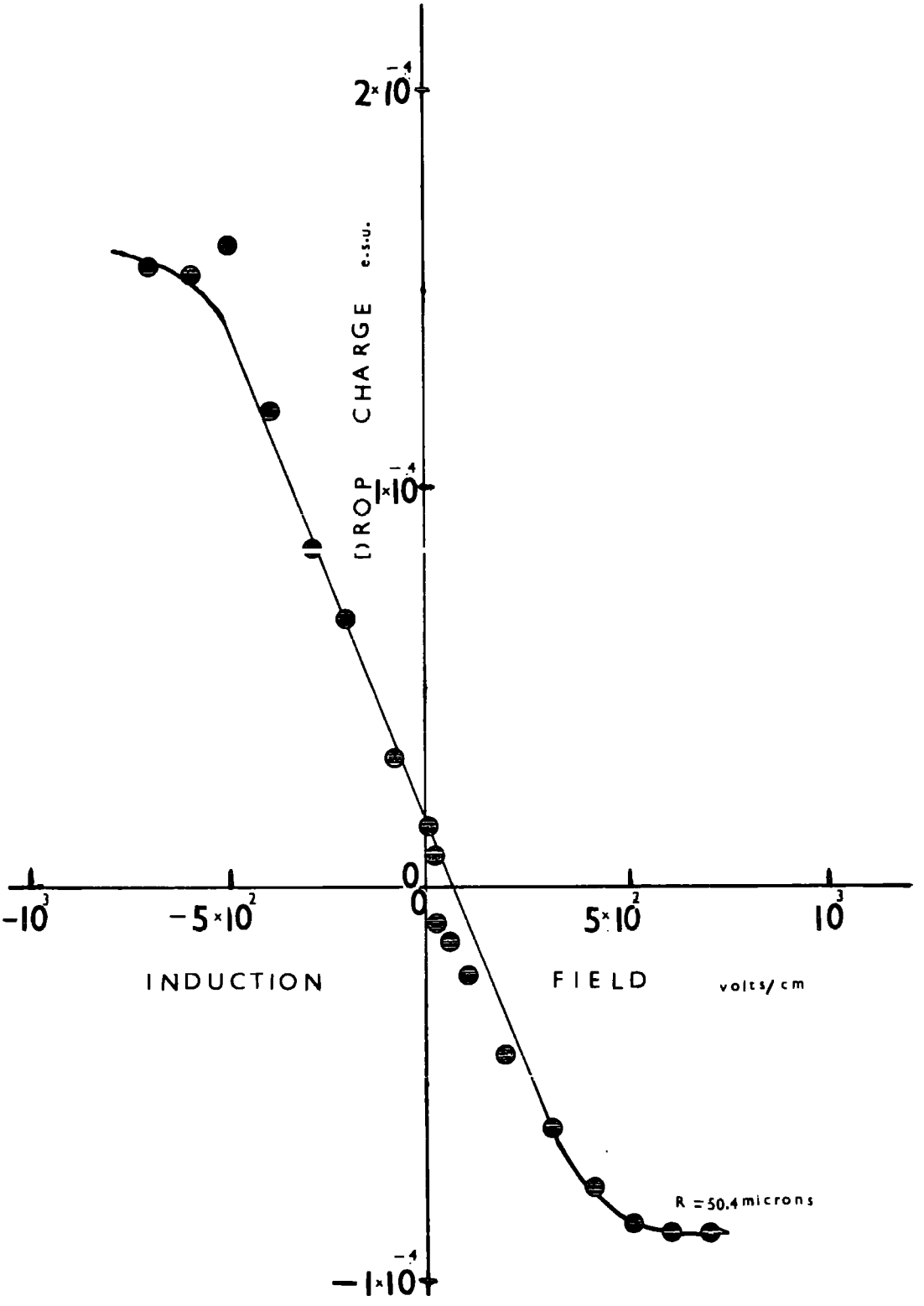

FIG. 4.14.
THE CHARGE OF THE TOP JET DROPLET RADIUS OF 75.6 MICROMETRES WITH INDUCTION FIELD FROM 0 TO $\pm$ 10 Vcm^{-1}.

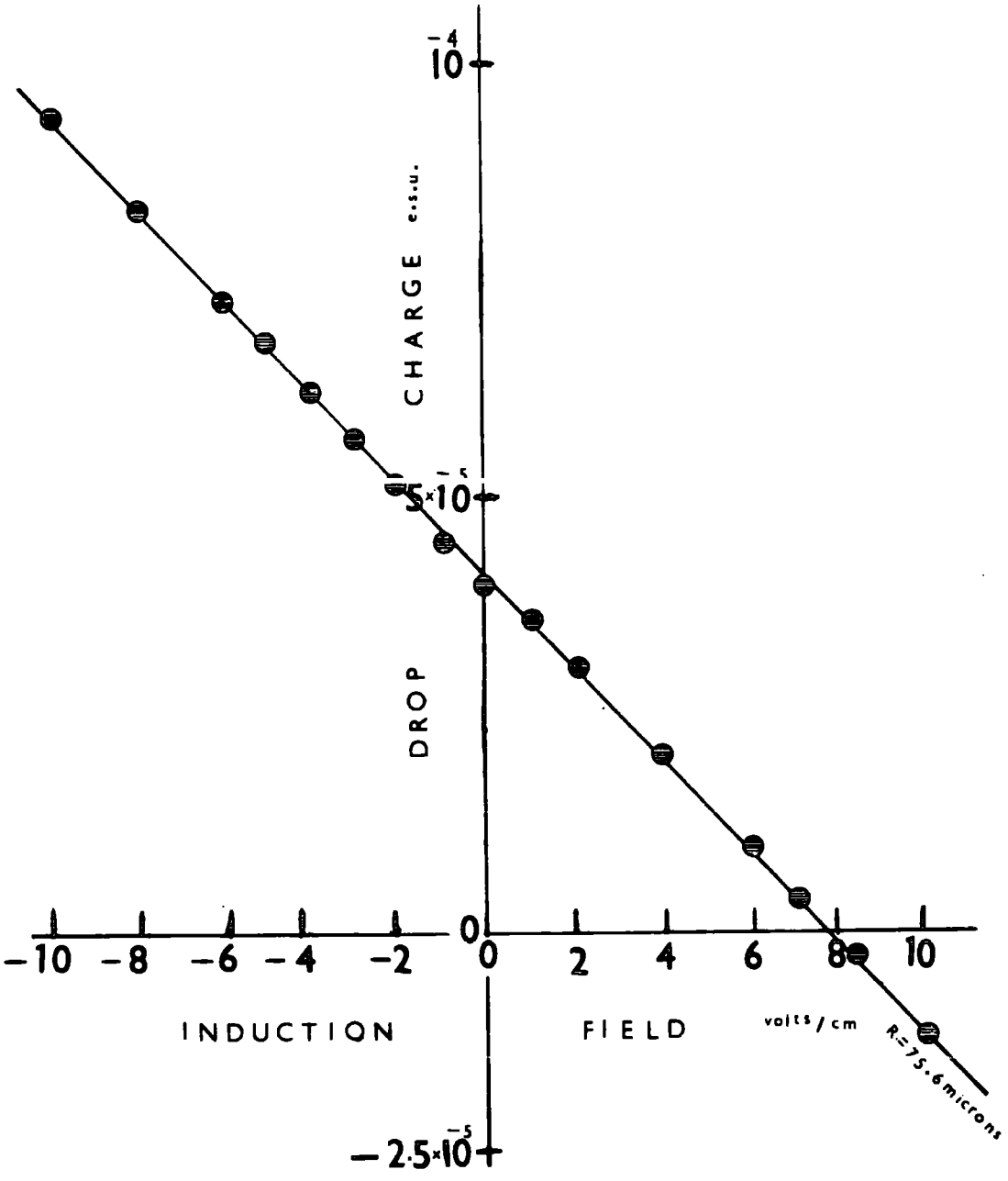

FIG. 4.15.
THE RELATION BETWEEN THE CHARGE OF THE TOP JET DROPLET RADIUS OF 75.6 MICROMETRES FOR THE RANGE 0 TO $\pm$ 90 V cm^{-1} OF INDUCTION FIELD.

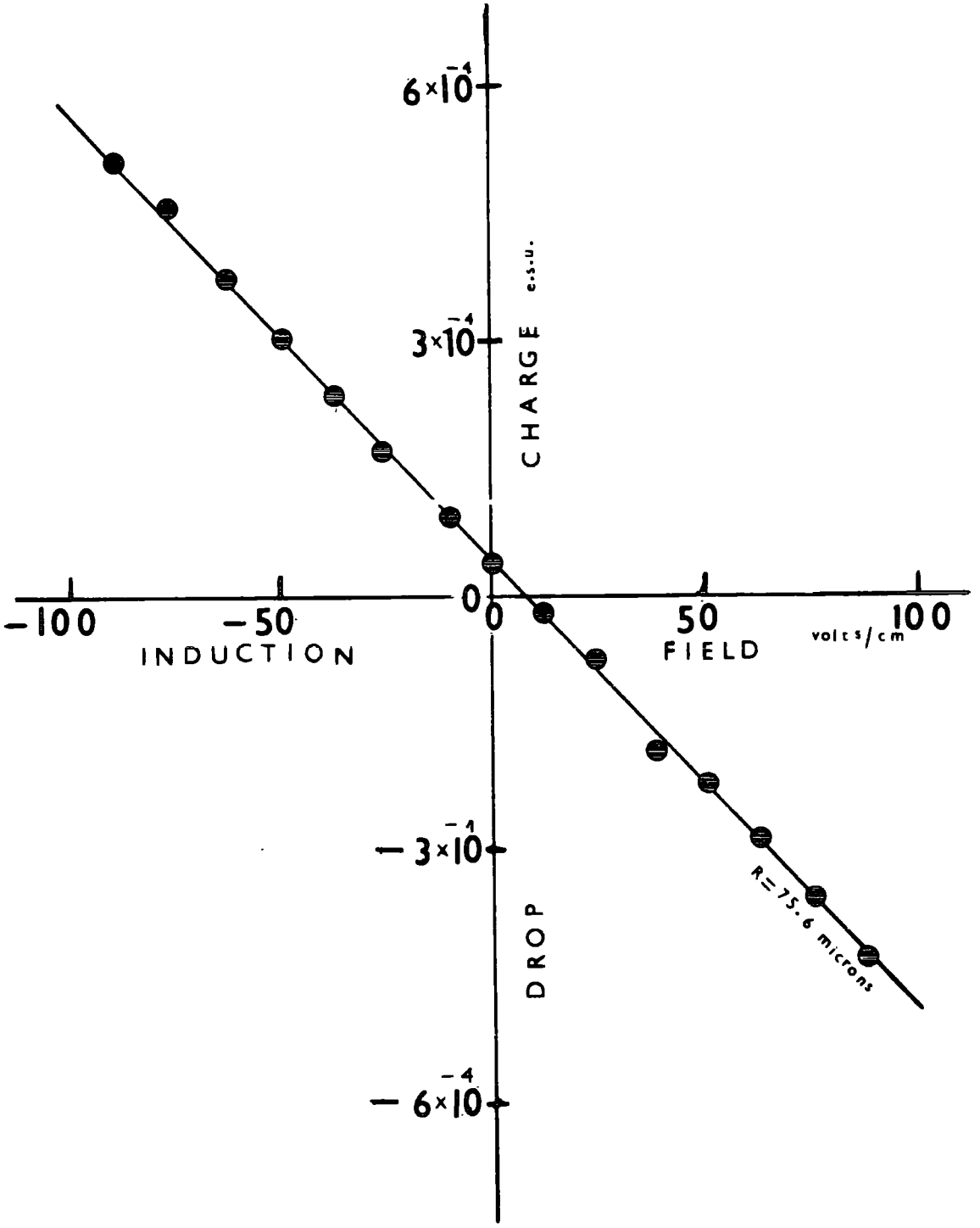

FIG. 4.16.
THE INDUCTIVE CHARGE ON THE TOP SEA-WATER DROPLET OF RADIUS 26.7 MICROMETRES FOR A RANGE OF 0 TO $\pm$ 25 V cm^{-1} FOR THE INDUCTION FIELD.

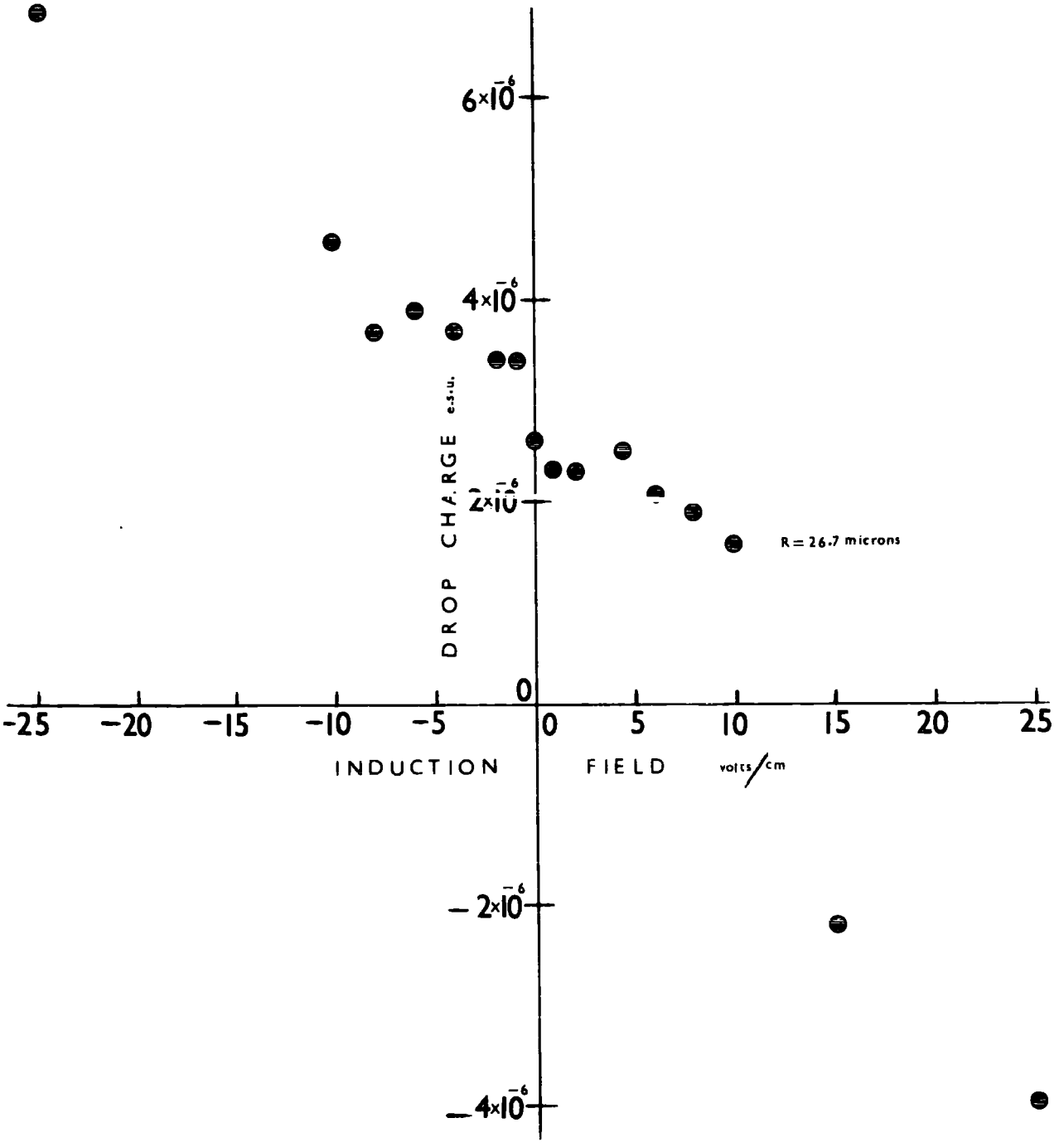

CHAPTER 5

DISCUSSION AND APPLICABILITY OF THE RESULTS

5.1. The Production of jet droplets.

It has been shown that jet droplets are produced by a bursting bubble at an air-water interface over a wide range of operating conditions. A relation of the form $D_d \propto D_B^{1.22}$ was determined over a range of bubble diameter D_B from 0.3 up to 3 mm corresponding to droplet diameters from about 35 up to 700 micrometres.

Woodcock (1953) found that relatively few bubbles greater than 1 mm diameter are present in the spectrum of bubble sizes produced at sea. This implies that the limiting size of jet droplets produced from sea-water, as indicated from the results of Chapter 3, is about 200 micrometres in diameter. A typical sample of jet droplets of average diameter 100.8 micrometres produced from a bubble of diameter 720 micrometres is shown in Fig.5.1. The droplets were impacted onto a magnesium coated slide under the influence of an electric field. The uniformity in size is typical of a top jet droplet spectrum measured in the described experiments. The experiments also indicate that a bubble diameter of a particular size produces approximately identically sized droplets for both distilled water and sea-water.

Measurements of ejection height of the top jet droplet demonstrates that almost identical heights are attained for distilled water and sea-water for bubble diameters less than about 1 mm in diameter. This result agrees with measurements made by Blanchard and Woodcock (1957) in sea-water and those of Stuhlman (1932) with distilled water. Salinity plays no

FIG.5.1. A PHOTOGRAPH OF A TYPICAL SAMPLE OF JET DROPLETS OF AVERAGE DIAMETER 100.8 MICROMETRES EMITTED FROM A BUBBLE OF DIAMETER 720 MICROMETRES.

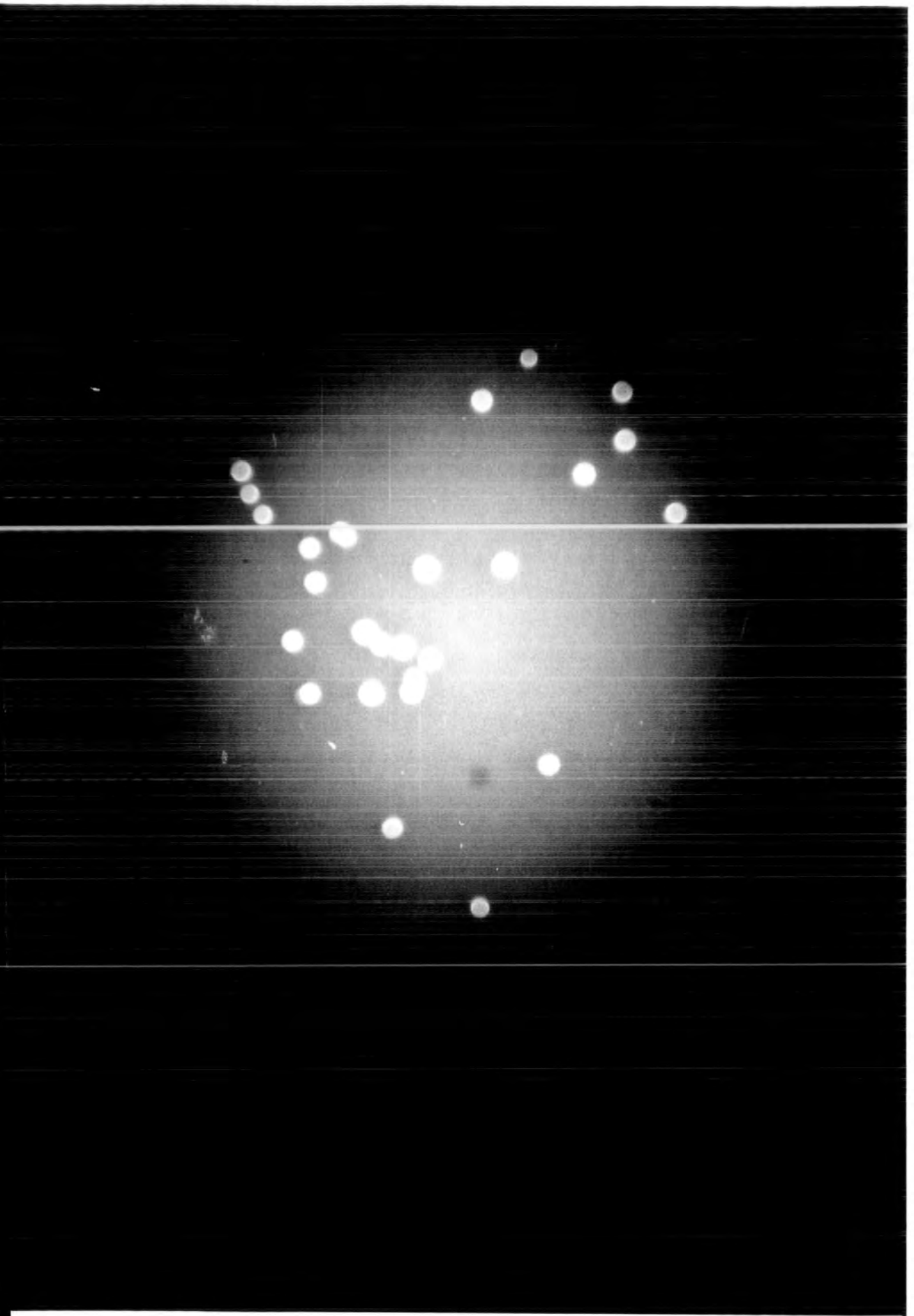

direct role in ejection height even for the larger bubbles. The difference in ejection heights for droplets produced from sea-water (greater height) and those from sea-water is mainly due to the longer time the bubble remains at the sea-water surface.

The bursting bubble produced on average from four to five jet droplets, each possessing a characteristic size and ejection height. Fig.5.2. shows a photograph of the trajectory of four jet droplets rising from a bubble bursting at an air-water interface. The maximum ejection height of the top jet droplet in Fig.5.2. is 8.2 cm. Deceleration of the droplet is caused by the frictional drag which is dependent on the droplet size and velocity. The free surface energy of the bubble is the main contribution to the kinetic energy of the droplets. Between ten and twenty per cent of this surface energy is normally converted into droplet kinetic energy, the remainder being converted into heat and capillary waves, as seen, for example in the high-speed photographs of Kientzler et al (1954).

It is considered that the production of jet droplets is one of the main sources of sea-salt nuclei. Film droplets is also a major source as discussed by Mason (1957) but this subject falls outside the scope of the present work. The production of jet droplets depends on the bubble spectrum which is a strong function of wind speed and temperature of the sea-water. Four measurements of the bubble size distribution with wind speed have been made. However, measured sea-salt spectra by Woodcock (1953) can be used to give a droplet spectrum by assuming that the salt particles originate from the jet droplets. This conversion has been made by Blanchard (1963) and the

FIG. 5.2. THE TRAJECTORIES OF THE FOUR JET DROPLETS FROM A BURSTING BUBBLE OF DIAMETER 720 MICROMETRES. EJECTION HEIGHT OF TOP DROPLET = 8.2 cm.

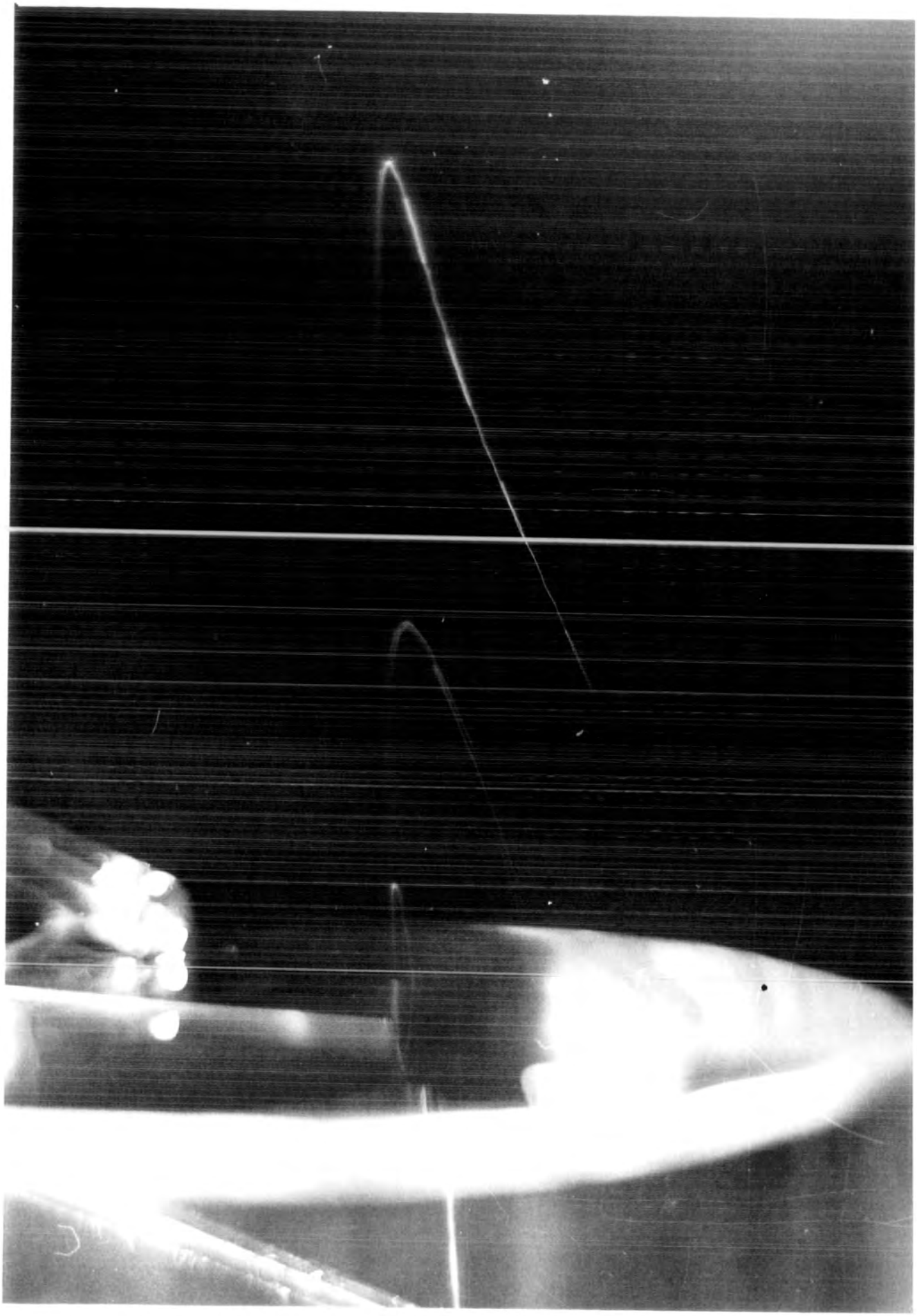

spectrum of droplets that must be produced by the sea to account for the observed sea-nuclei corresponds quite well with the jet droplet size range produced from bubbles up to about 600 micrometres in diameter measured in the laboratory.

The technique of jet droplet production from bursting bubbles can be used to provide an alternative method of droplet generation over a size range from about 15 up to 350 micrometres in radius. In addition, since the jet droplet height is quite reproducible the particular technique could be usefully employed in precise liquid drop-collision studies.

5.2. Discussion of the natural charge of the jet droplets

It was found that the jet droplets always carried a positive charge. The lowest value of water conductivity used in the experiments was about 2.8 μ mho's cm^{-1}. The charge polarity agrees with the results of Blanchard (1963) for a similar range of water salinity. For lower salinity of the order of 0.1 and 0.02 ppm NaCl, Blanchard found negative charging of the jet droplets. No experiments were carried out on water possessing such low salt concentrations.

A schematic representation of the charge distribution which is assumed to exist within a bubble jet at the moment the jet droplets are formed is given by Blanchard (1963) and is shown in Fig.5.3. An electrical double layer is assumed to exist at the liquid surface with the negative layer nearest the surface. Using the hypothesis that laminar flow conditions are fulfilled in the jet, then the liquid at the core of the jet will move fastest. Therefore the positively charged central core will be transported quicker up through

FIG. 5.3.
A DOUBLE-LAYER CHARGING THEORY FOR JET DROPLETS.

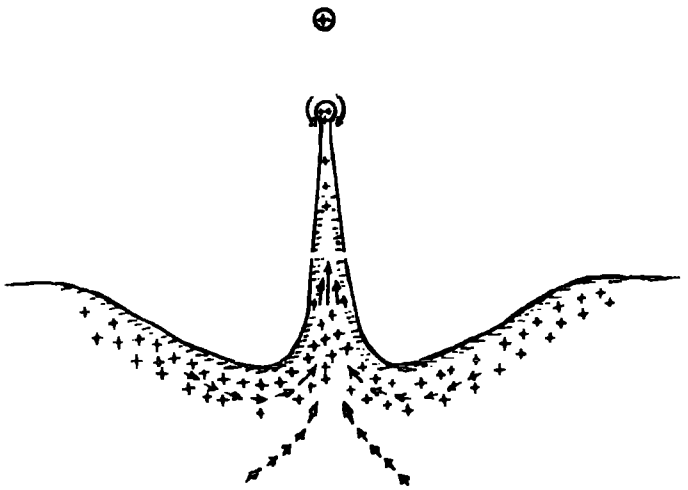

the jet than the slower moving negatively charged region near the jet surface. Hence, a net positive charge appears in the jet droplets as they break away from the jet under the influence of surface tension forces. However, more work is required to validate the laminar flow assumption within a bubble jet. This could be explored through the use of dye tracers in the liquid combined with high speed photography of the emerging jet.

The magnitude of the electric charge was estimated from Equation 2.1. The largest error in q arises from errors associated with the measurement of R. Usually a droplet count of between 10 and 15 was used to estimate the mean droplet size. In addition, a mean value of electric field was calculated from about 10 readings for easier charge determination.

It was found that the jet droplet charge generally increased with the bubble age, as indicated by the experimental results of Figs. 4.3. and 4.7. respectively. A typical percentage increase in droplet charge of about 30 per cent was found for a droplet radius of 30 micrometres as the bubble age increased from 0.3 to 6 seconds. A straight line relation of charge, q, versus bubble age, t, gave a result of $q \propto t^{0.28}$ for droplets of radius 36 micrometres. This gives reasonable agreement with experiments carried out by Blanchard (1963) on droplets less than about 20 micrometres in radius.

The dependence of the droplet charge on the bubble age suggests that the droplet charge is associated with a change in the bubble itself which is known to be time dependent under certain conditions. Alty (1926) found that the charge on the bubble increased to a maximum with bubble age then decreased to an equilibrium value. He also found that the

equilibrium charging time decreased with increasing conductivity of the water. The experiments described in Chapter 4 agree with Alty's finding of charge increase with bubble age. However, the age experiments were not extended beyond a bubble age of 8 seconds, so that equilibrium charging conditions were not attained.

5.3. Variation of the natural droplet charge with water conductivity.

Results of droplet charge versus water conductivity showed that the droplet charge increased by about a factor of 3, for constant bubble ages of 0.3, 4 and 7 seconds, as the water conductivity was decreased by about four orders of magnitude. These results were shown in Fig. 4.10. A reduction in the salt solution concentration (decrease in the conductivity) from the sea-water value by about an order of magnitude produced no significant effect on the droplet charging.

The rate of charging of a liquid drop, $\frac{dQ}{dt}$ is approximated by Iribarne and Klemes (1974) by the expression:

$$\frac{dQ}{dt} = I - i \qquad (5.1.)$$

where I is the net charge carried by the liquid in unit time. The current, I, results from the shearing of the diffuse part of the electrical double layer existing at the neck of the liquid jet. The accumulation of charge, Q, on the drop of radius R produces an electric field of $\frac{Q}{\varepsilon_{R^2}}$ where ε is the dielectric constant of the liquid. Therefore, the current i which opposes the main charging I is given by:

$$i = \frac{\pi r^2 D.K.}{\varepsilon R^2} \qquad (5.2.)$$

where K is the liquid conductivity and r is the radius of the neck of the jet. The charging current I has been shown by Iribarne (1972) and Iribarne and Klemes (1974) to be equal to:

$$I = - \frac{\varepsilon T \zeta}{8 \eta} \qquad (5.3.)$$

where T is the surface tension of the liquid, η the viscosity of the liquid and ζ is the electrokinetic potential at the air-liquid interface which possesses a value of approximately - 1.2×10^{-4} stat V according to Bach and Gilman (1938).

A family of curves have been plotted (a) for three values of jet droplet radii of 2, 20 and 200 micrometres respectively and (b) for two values of the ratio r_o/a of 0.1 and 0.3 respectively, where a is the initial radius of the undisturbed jet of liquid which emerges from the collapsing bubble and r_o is equal to the initial filament radius. The parameters, R, a and r_o are defined in Fig.5.4. Photographs of liquid jet breakups suggest values for r_o/a between 0.1 and 0.3

The numerical integration of Equation 5.1. together with the substituted values of expressions 5.2. and 5.3. yield a series of curves of droplet charge q versus conconductivity K which have been derived by Iribarne and Klemes (1974) and are shown in Fig.5.5.

Experimental values of droplet charge q (see Fig.4.10) are also plotted in Fig.5.5. The experimental results obtained in Chapter 4 can be compared with the predicted values of Iribarne and Klemes because at these high conductivities the droplet charging can be attributed to the mechanism studied here.

FIG. 5.4.
FORMATION OF A JET DROPLET OF RADIUS R FROM COCYLINDRICAL LIQUID JET OF INITIAL RADIUS, a.

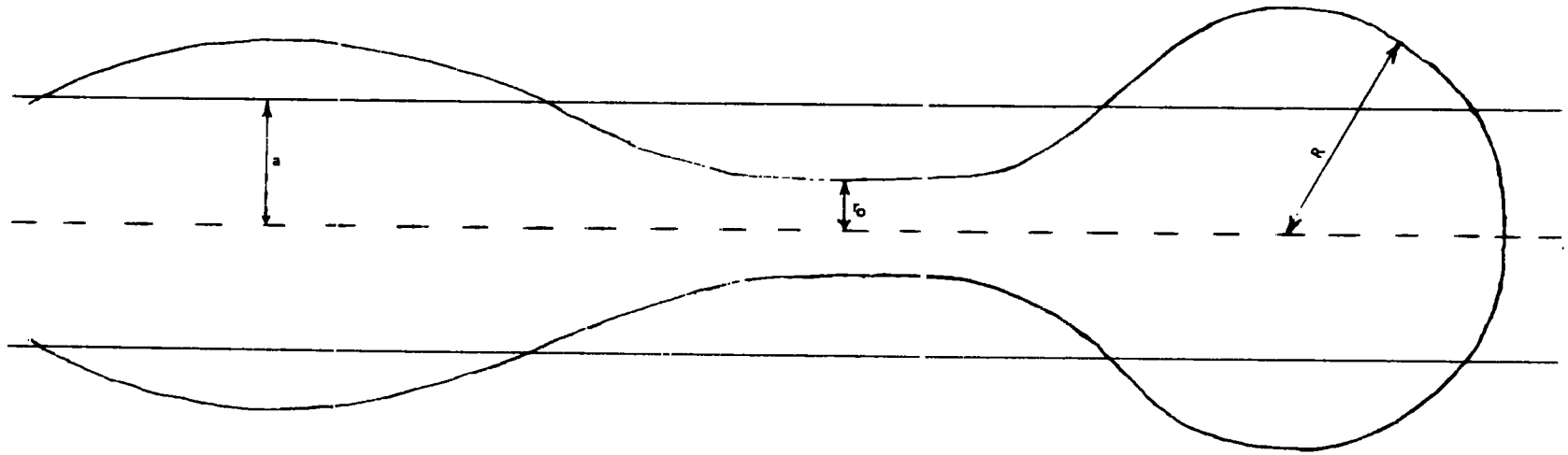

FIG. 5.5.
THEORETICAL JET DROPLET CHARGE AS A FUNCTION OF THE LIQUID CONDUCTIVITY.
Experimental points are represented as follows:
●. ●, o Droplets 19.2 micrometres radius and 0.3, 4, 6 seconds of bubble age respectively.
▲ o Droplets 27.5 micrometres radius and 0.3, 6 seconds of bubble age respectively.
X Droplets 66.8 micrometres radius and 0.3 seconds of bubble age.

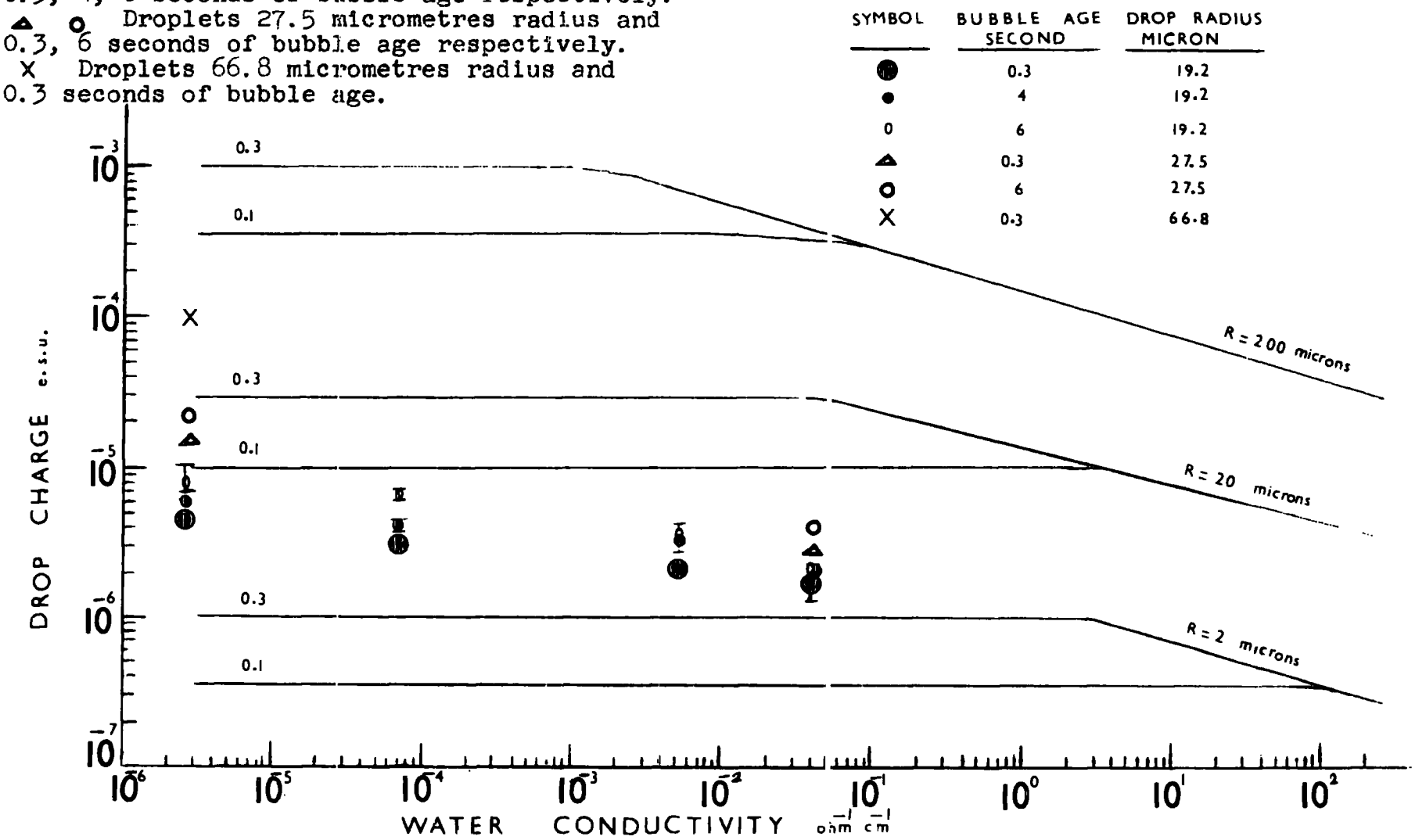

It can be seen that the experimental results for jet droplets of 20 micrometres in radius are close to the predicted values for the lower values of liquid conductivity, and are within a factor of between three and four for liquid conductivity greater than about 10^3 μmho's cm^{-1}. The comparison can be regarded as showing reasonably good agreement with the electrical double layer-charge shearing theory. Other experimental values obtained for larger jet droplets for both low conductivity (between 2 and 3 μmho's cm^{-1} for deionized water) and for sea-water of conductivity 4×10^4 μmho's cm^{-1} are shown also in Fig.5.5. Agreement with prediction is seen to be reasonably good up to values of droplet radius of about 70 micrometres.

The present theory does not concur with the decrease in droplet charge for jet droplets with radii greater than about 70 micrometres as shown in Fig.4.6. A possible explanation for the decrease in the top droplet charge above a critical droplet size is given below.

Blanchard (1963) has computed the top droplet ejection speed as a function of bubble size through the application of the normal gravitational force and frictional retarding force on the droplet. The relation between the drop ejection speed and top droplet radius is shown in Fig.5.6. The values of droplet radii have been obtained from the measured relation between the bubble size and jet droplet radius of Fig.3.6. The result of Fig.5.6. shows that the ejection velocity of droplets decreases with increasing droplet size. This result is also supported by the relation between the drop ejection height versus the droplet radii as shown in Figs.3.2.

FIG. 5.6.
TOP JET DROPLET EJECTION VELOCITY AS A FUNCTION OF DROPLET RADIUS.

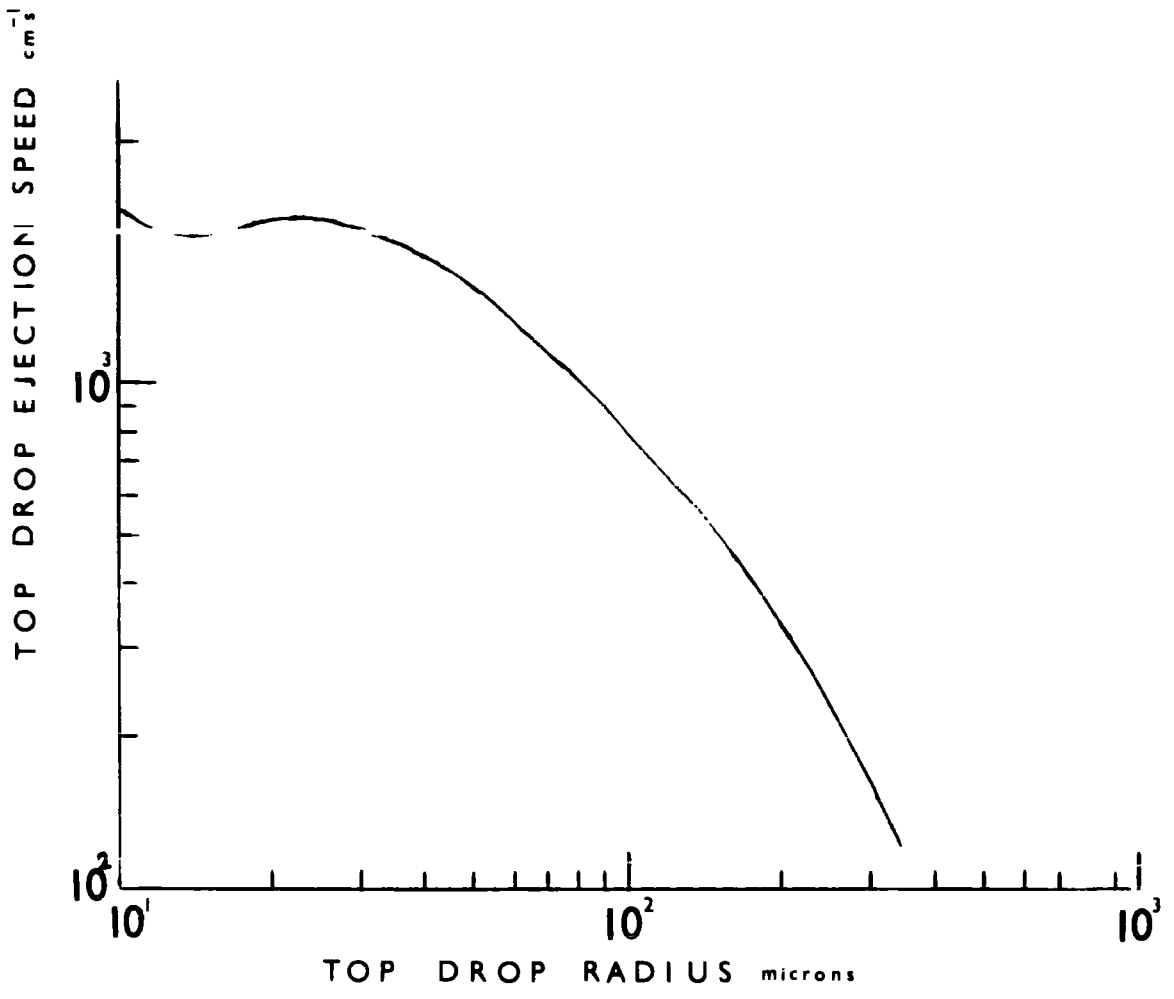

Although precautions were taken to have the deionized water and sea-water samples free from impurities, nevertheless it is likely that the deionized water probably became contaminated with organic substances during their storage in the glass reservoir. This probably occurred because the elimination of natural organic, surface-active films requires extreme caution and care in maintaining the liquid free from natural room air contaminants.

The rate of renewal of surface organic material is inversely proportional to the ejection velocity of the jet droplet. This is consistent with the work of Blanchard (1963) who found that the efficiency of film removal increases with an increase in bubble size. He found that negligible surface contamination was carried away by the top droplet for bubble diameters less than about 1 mm, but found that for a 2.6 mm diameter bubble, the top droplet's surface area was completely covered with a film coating.

It is well established that the presence of an organic film or contaminants on a liquid droplet surface reduces the electric charge on the droplet. Limited experiments by Blanchard suggested a reduction in the droplet charge through the effect of surface active contamination films on the bulk sea-water. It is considered that the reduction in the charge carried by jet droplets of radius greater than about 70 micrometres could be partly due to the described effects, namely (i) an increase in the attachment of film contaminants into the jet droplet surface as the jet droplet ejection velocity increases with increasing size, as seen in Fig.5.6., and (ii) the reduction in droplet charge with increase in surface impurities on the droplet. Controlled experiments are

required to establish in more quantitative terms the relation between surface film contaminants and droplet charge.

5.4. Discussion of the inductive charging experiments.

Numerous induction charging experiments were carried out both for distilled water and sea-water. Operating electric fields for a small range from 0 to $\pm$ 10 V cm^{-1} and for the larger range from 0 to $\pm$ 175 V cm^{-1} were used. Larger electric fields up to 700 V cm^{-1} were used in experiments on the second jet droplet. Experiments were carried out on jet droplets ranging in radii from 26 up to 76 micrometres.

A linear relation between droplet charge and induction field was found in all experiments conducted. The age of the bubble had no effect on the inductive charge, as expected. An applied electric field of + 90 V cm^{-1} was necessary to neutralize the top jet droplet of radius 36 micrometres for distilled water compared to a value of about 12 V cm^{-1} for sea-water droplets of radius 27 micrometres.

The neutralization of the sea-water droplet is probably unlikely to occur since the large requisite electric field of about 12 V cm^{-1} is usually associated with disturbed weather conditions which usually give negative field values. This would induce a positive charge on the droplets, thus increasing the natural positive charge of the droplet. It is also probable that the large (negative) electric fields at the sea-surface caused by oceanic thunderstorms will induce positive charges on the jet droplets considerably in excess of their natural charge. For example, the experimental results shown in Fig. 4.12 indicate an increase of the induced positive charge by a factor of 2 for a negative field of 76 V cm^{-1}.

The induced charge on the second jet droplet was about a factor of 8 less than for the top jet droplet of near equivalent size, as seen in Fig. 4.11. This is contrary to the results of Blanchard (1963) who found that induction charging exerted a relatively greater influence in the second drop.

It may be concluded that the negative charge which would be induced in the top droplet by the earth's fair-weather electric field of about 2 V cm^{-1} constitutes only a small fraction (and opposite) to the natural charge in the droplets. The reduction in the natural charge of the top droplet due to an applied positive potential of 2 V cm^{-1} for droplets of radii 27 micrometres (sea-water), 36 micrometres (distilled water), 46 micrometres (distilled water) and 76 micrometres (distilled water) is 9, 3, 2 and 25 per cent respectively.

The first report of electrical charging during the melting of ice was made by Dinger and Gunn (1946). The charging associated with the bursting of bubbles in dilute water is of great interest in connection with the electrification of melting ice and snow, since it is known that large numbers of tiny air bubbles are released during the melting process. Iribarne and Mason (1967) found that droplets ejected from pure water and water solution less than 10^{-4} M (less concentrated than what was used in this work) carried a negative charge and a positive charge for more concentrated solutions. Drake (1968) found strong positive charging for highly purified ice specimens melting. The onset of charging considered coincided with the initiation of convective currents in the melt water which gave rise to the formation of bubbles in the

melt-water. His results of decreasing charge with increasing concentration of specimen solutions of ice agree with the experimental results obtained for jet droplets emerging from liquids of varying conductivity in Chapter 4. The study of droplet charging from bursting bubbles can also be applied to the charge separation that may occur at the surface of a raindrop which is in process of melting from a snow-flake or hailstone. It is now well established that the interior of large hailstones contains rings of air bubbles, as discussed by Mason (1971). It is likely that a melting snow-flake or hailstone produces numerous air bubbles that eject charged jet droplets into the air, the sign and magnitude of which is very sensitive to the size and age of the bubbles and to the purity of the precipitation particles.

ACKNOWLEDGEMENTS.

I would like to take this opportunity to give thanks to the persons who offered aid, encouragement and advice as this work progressed. Firstly, to Dr. S.G. Jennings, for his sincere appreciation of the suggestion of the project, his supervision and constant advice, and to Professor A.W. Wolfendale the Head of the Physics Department.

I am indebted to all members of the Atmospheric Physics Group, and in particular to Mr. Jack Moralee for the construction of the apparatus. Mr. John Scott is thanked for his drawing of the jet tube and for building the glass apparatus. Mrs. M. Kimmitt is thanked for the speed and efficiency with which she typed this thesis.

I would also like to thank my country, Saudi Arabia, and in particular the Military College.

REFERENCES

Alty, T., (1926) — Origin of the electric charge on small particles in water. Proc. Roy. Soc., London (A), 112, pp. 235-251.

Bach, N., and Gilman, A., (1938) — 'The electrokinetic potential at gas-liquid interfaces. I. The cataphoretic velocity of gas bubbles in solutions of inorganic electrolytes'. ACTA Physicochimica, URSS, 9, pp. 1 - 26.

Blanchard, D.C., (1955) — Electrified droplets from the bursting of bubbles at an air-sea water interface. Nature, 175, pp. 334-336.

Blanchard, D.C., (1958) — Electrically charged drops from bubbles in sea-water and their meteorological significance. J. Meteor. 15., pp. 383-396.

Blanchard, D.C., (1963) — The electrification of the atmosphere by particles from bubbles in the sea. Progress in Oceanography, 1, pp.71-202.

Blanchard, D.C., and Woodcock, A.H., (1957) — Bubble formation and modification in the sea and its meteorological significance. Tellus, 9, pp. 145-158.

Day, J.A., (1964) — Production of droplets and salt nuclei by the bursting of air bubble films. Q. Jl. R. Met. Soc., 90, p.72-78.

Drake, J.C., and Mason, B.J., (1966) — 'Melting of small ice spheres and cones'. Q. Jl. R. Met.Soc., 92, p.500.

Drake, J.C. (1968) — "Electrification accompanying the melting of ice particles", Q. Jl. R.Met.Soc., 94, p.176.

Iribarne, J.V., and Mason, B.J., (1967) — Electrification accompanying the bursting of bubbles in water and dilute aqueous solutions. Trans. Farad. Soc., 63, pp.2234-2245.

Iribarne, J.V. and Klemes, M., (1974) — Electrification associated with droplet production from liquid jets. J. Chem. Soc., Faraday Trans.I., 70, pp.1219-1227.

Kientzler, C.F., Arons, A.B., Blanchard, D.C., and Woodcock,A.H., (1954) — Photographic investigation of the projection of droplets by bubbles bursting at a water surface. Tellus, 6, pp. 1 - 7.

Mason, B.T., (1957) — The oceans as a source of cloud-forming nuclei. Pure and Applied Geophysics, 36, pp. 148-155.

Mason, B.J., (1971) — The Physics of Clouds, Clarendon Press, Oxford.

May, K.R., (1950) — The measurement of airborne droplets by the magnesium oxide method. J. Scient. Instrum. 27, pp.128-130.

May, K.R., (1965) — A new graticule for particle counting and sizing. J. Scient. Instrum. 42, pp. 500-501.

Newitt, D.M., Dombrowski, N., and Knelman, F.H., (1954) — The mechanism of drop formation from gas or vapour bubbles. Trans. Inst. Chem. Engrs. 32, pp. 244-261.

Stuhlman, O., (1932) — The mechanics of effervescence. Physics, 2, pp.457-466.

Woodcock, A.H., (1953) — Salt nuclei in marine air as a function of altitude and wind force. J. Met., 10, pp.362-371.

Woodcock, A.H., Kientzler, C.F., Arons, A.B., and Blanchard, D.C., (1953) — Giant condensation nuclei from bursting bubbles. Nature, 172, pp. 1144.